

# We are IntechOpen, the world's leading publisher of Open Access books Built by scientists, for scientists

6,900

Open access books available

186,000

International authors and editors

200M

Downloads

Our authors are among the

154

Countries delivered to

TOP 1%

most cited scientists

12.2%

Contributors from top 500 universities



WEB OF SCIENCE™

Selection of our books indexed in the Book Citation Index  
in Web of Science™ Core Collection (BKCI)

Interested in publishing with us?  
Contact [book.department@intechopen.com](mailto:book.department@intechopen.com)

Numbers displayed above are based on latest data collected.  
For more information visit [www.intechopen.com](http://www.intechopen.com)



# Effect of Applying Ultrasonic Vibration in Hot Embossing and Nanoimprint

Harutaka Mekarū

*National Institute of Advanced Industrial Science and Technology (AIST)  
Japan*

## 1. Introduction

Nanoimprint lithography (NIL) is a technology where fine structures on a mold (or template) are transferred onto a substrate coated with thermoplastic or with ultraviolet (UV) curing resins by making contact with the substrate while being heated or exposed to UV lights. Recently, NIL has been applied in semiconductor manufacturing to print fine features of circuits on LSI chips and memories at reduced manufacturing cost. Current nanoimprint technology can be classified as thermal nanoimprint and UV nanoimprint.

In thermal nanoimprint, a mold is heated to above the glass transition temperature ( $T_g$ ) of a thermoplastic while keeping the mold pattern pressed against the thermoplastic by applying a loading force, as shown in Fig. 1(a). After keeping the mold and the thermoplastic in that position for a while, they are then cooled down to below the  $T_g$ , and the mold is then released from the solidified thermoplastic. In this technique, depending on thermal deformation, there is a likelihood of deterioration of the positional accuracy and the shape of the pattern. Moreover, the total processing time in thermal NIL also becomes long.

On the other hand, in the case of UV nanoimprint, a template made of material with quartz-like UV-transparency, is brought into contact with a substrate coated with a UV-curing resist. The step is then followed by UV irradiation of the UV-curing resist through the template, as shown in Fig. 1(b).

We are developing a nanoimprint technology for the replication of patterns that employs ultrasonic vibration instead of thermal cycling or UV radiation. In this technique, by maintaining a pressure between mold patterns and thermoplastic, a certain amount of heat is generated at their interface by inducing ultrasonic vibration where the patterns are transformed thermally as shown in Fig. 1(c). In thermal nanoimprint, the molding material is heated to above its  $T_g$ , followed by a time consuming process of thermal cycling using electric or oil heating. The use of ultrasonic vibration for the generation of heat had also been proposed in thermal nanoimprinting. However, during the heating, a large amount of energy is lost into the mold material exposing it to mechanical stress. In the present work, the mold is mounted on an ultrasonic generator where the vibration is impressed in a direction of pressure applied on the thermoplastic. Here the mold patterns are pushed and pulled very rapidly within the surface of the thermoplastic. Therefore, the temperature of the mold hardly changes from the room temperature. Here, an assisting effect of ultrasonic vibration in hot embossing and in thermal nanoimprint is shown in a time series which also describes the processes of ultrasonic nanoimprinting.

Source: Lithography, Book edited by: Michael Wang,  
ISBN 978-953-307-064-3, pp. 656, February 2010, INTECH, Croatia, downloaded from SCIYO.COM

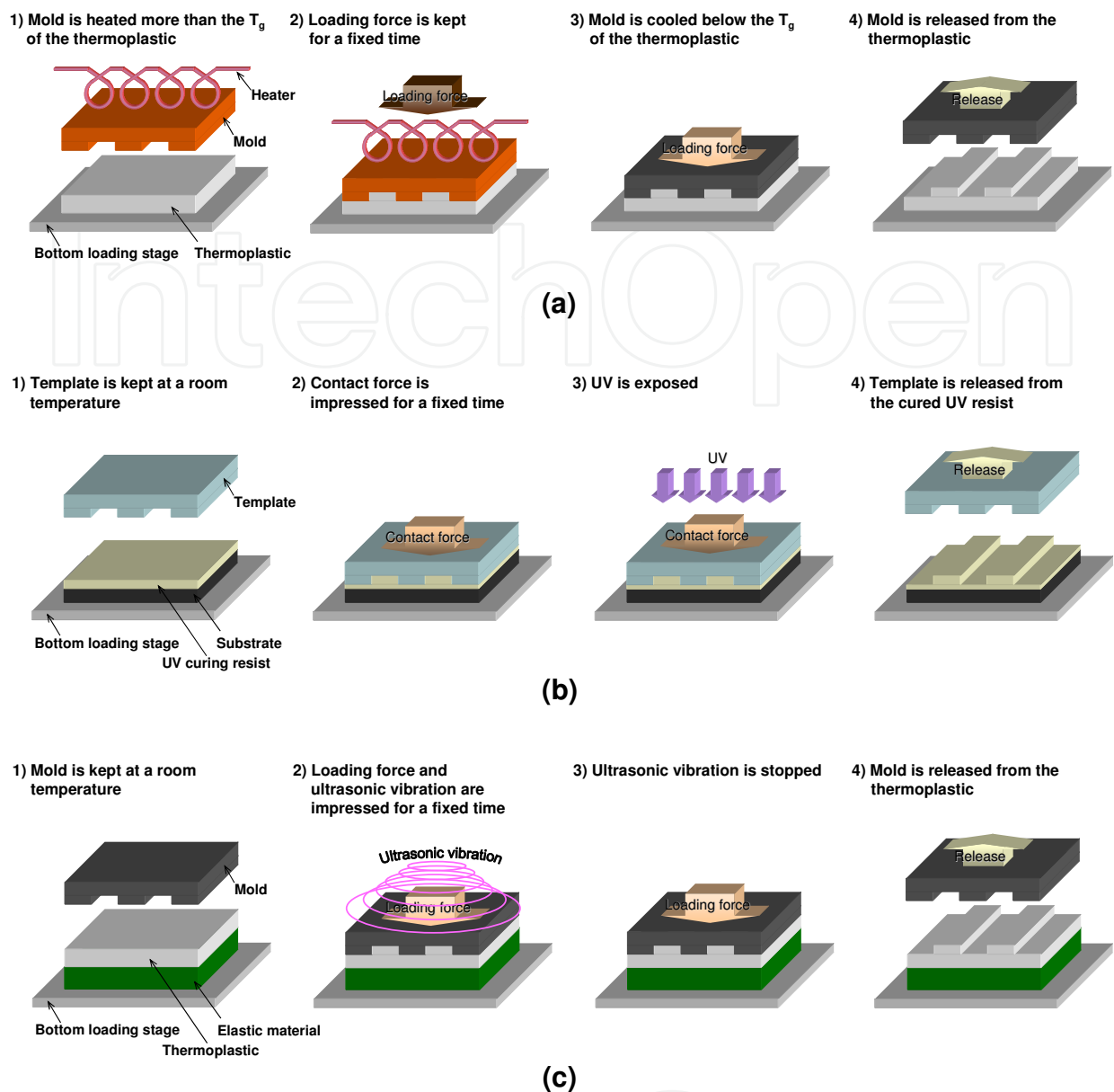


Fig. 1. Concept of process flows in (a) thermal nanoimprint, (b) UV nanoimprint, and (c) ultrasonic nanoimprint.

2. Hot embossing assisted by ultrasonic vibration

2.1 In case of impressing ultrasonic vibration with high amplitude

The introduction of ultrasonic vibration into replication technologies has led to the development of a molding technique for achieving high-aspect ratios (aspect ratio = pattern depth/ width of the pattern). As a technique for fabricating the microstructure of the high-aspect ratio, LIGA (Lithographie, Galvanoformung and Abformung) process is widely known. The LIGA process is a total processing technology that combines X-ray lithography, with electroforming, and molding. X-ray from a synchrotron with its high permeability and directivity is irradiated on a thick resist to form structures with high-aspect ratios. The resist structure is then transformed into a metallic mold processed by electroforming. Electroformed metallic structures are used as mold patterns to mass produce high-aspect-

ratio replicated structures in thermoplastic such as in hot-embossing. However, because of trapped air/ gas in the cavity of mold pattern the softened molding materials cannot fully enter into it, resulting in the formation of defective imprinted patterns with reduced aspect ratios. Although this problem has been addressed by hot embossing in vacuum but because of the accompanying decompression/ purge operation and heating/ cooling cycle in an insulated environment of vacuum, the process takes more time. Then, the author thought of assisting the flow of softened material into the mold pattern by applying ultrasonic vibration in hot embossing at room atmosphere.

A new vacuum hot embossing system was developed at University of Hyogo. The maximum pattern size that could be embossed was  $50 \times 50 \text{ mm}^2$ , at a maximum available temperature of  $400^\circ\text{C}$  at which most thermoplastics and sealing glasses are embossed. A servomotor with a maximum output of 50 kN was used in this system. As a result, positional accuracy and pressing speed of the loading stage can be precisely controlled.



Fig. 2. (a) Photograph of an ultrasonic hot embossing system, and (b) bottom loading stage based on an ultrasonic horn.

In this research, a piezoelectric actuator was built into a vacuum hot embossing system as an ultrasonic vibration generator, and the effect of assistance by the ultrasonic vibration in hot embossing was verified experimentally. Figure 2 shows a setup of an ultrasonic vibration generator installed in the hot embossing system. The bottom loading stage installed in the heater of the vacuum hot embossing system was detached, and a longitudinal 15 kHz ultrasonic vibration generator USV-900Z15S (Ultrasonic Engineering Co., Ltd.) with  $16 \pm 2 \mu\text{m}$  amplitude and 900 W output was installed.

The metallic mold for the experiment was made by Si dry etching and Ni electroforming. The pattern was in shape of a hollow pyramid with a cut-out apex. There were five kinds of pattern entrances differing in lengths ranging from 100 to  $540 \mu\text{m}$ . All patterns had the same depths of  $260 \mu\text{m}$  and inclined sidewalls with curved surfaces. Figure 3 shows a photograph and details of the pattern size of the Ni mold measured with a three-dimensional (3D) laser microscope VK-9700 (Keyence Corp.). A polycarbonate (PC) was selected for the molding material. The  $T_g$  of PC is  $144^\circ\text{C}$ .

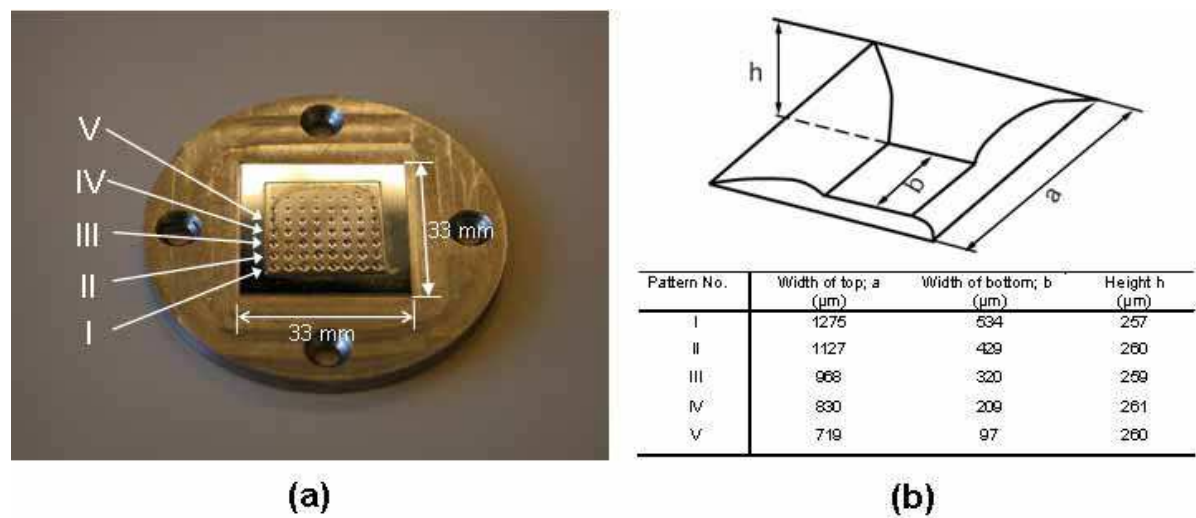


Fig. 3. Photograph of electroformed -Ni mold and details of measured pattern size.

The best molding conditions in the vacuum hot embossing were: mold temperature  $T_h = 180\text{ }^{\circ}\text{C}$ , contact force  $F = 0.5\text{ kN}$ , and contact time  $t = 60\text{ s}$ . Figure 4(a) shows a scanning-electron-microscope (SEM) image of the embossed pattern under these conditions. The Roman numerals I through V in this figure correspond to the size of the Ni mold pattern in Fig. 3, where the numeral I being of the largest and V of the smallest size. In the ultrasonic hot embossing, the conditions where the contact time could be shortened to  $t = 95\text{ s}$ , were  $T_h = 180\text{ }^{\circ}\text{C}$ , and  $F = 1.75\text{ kN}$ ; the conditions where the contact force could be reduced to  $F = 1.0\text{ kN}$ , were  $T_h = 180\text{ }^{\circ}\text{C}$ , and  $t = 150\text{ s}$ ; and the conditions for high reproducibility were  $T_h = 180\text{ }^{\circ}\text{C}$ ,  $F = 1.5\text{ kN}$ , and  $t = 150\text{ s}$ . Figure 4(b) shows the SEM image of the embossed pattern under these conditions of high reproducibility. The resin completely fills to the edge part of the mold pattern, and it can be confirmed that the molding accuracy of the ultrasonic hot embossing reached to the same level as in the vacuum hot embossing. On the other hand, if the ultrasonic vibration were not applied when other molding parameters were same as Fig. 4(b), it would not be possible to mold at all, as shown in Fig. 4(c). Even signs of the molded pattern could not be observed from patterns III to V by the SEM observation. As a result, the assistance of the ultrasonic vibration influencing the molding accuracy became apparent. However, there were one set of conditions e.g.,  $T_h = 200\text{ }^{\circ}\text{C}$ ,  $F = 5.0\text{ kN}$ , and  $t = 1,800\text{ s}$  (30 min) where molding could be carried out, although barely, without the use of ultrasonic vibration as shown in Fig. 4(d). Moreover, it turned out that when the contact force was too large in the ultrasonic hot embossing, the overload disturbed the spread of the ultrasonic vibration, and the molding accuracy worsened. Figure 4(e) shows the SEM image of the embossed pattern when the contact force  $F$  was set to  $4.0\text{ kN}$ , while other parameters being same as in Fig. 4(b). Based on these results, molding conditions giving excellent molding accuracies are plotted in Fig. 5. Here the contact force  $F$  (kN) and contact time  $t$  (s) are plotted along the horizontal and vertical axes. Molding conditions in the atmospheric hot embossing were plotted in the upper right of the figure; and molding conditions in the vacuum hot embossing are plotted in the lower left of the figure. This figure shows that molding conditions of both methods are quite separate from each other. However, both the contact force and contact time could be greatly reduced by adding ultrasonic vibration even in the room atmosphere. In fact, by employing ultrasonic vibration the contact force and contact time have been reduced to 1/ 3



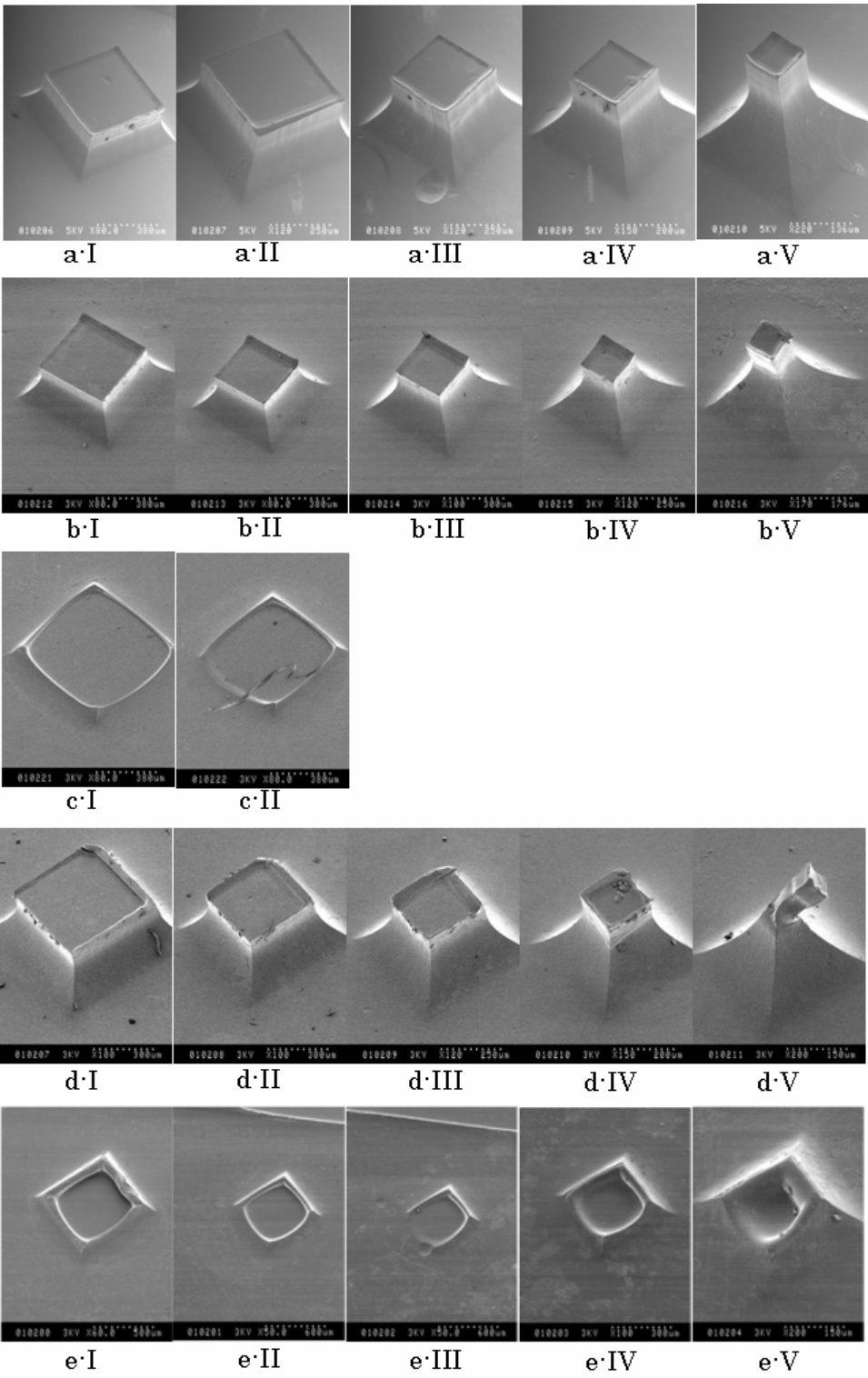


Fig. 4. SEM image of molded pattern (pattern size: I - V) under various conditions: (a) Vacuum hot embossing ( $T_h=180\text{ }^{\circ}\text{C}$ ,  $F=0.5\text{ kN}$ ,  $t=60\text{ s}$ ); (b) Ultrasonic hot embossing ( $T_h=180\text{ }^{\circ}\text{C}$ ,  $F=1.0\text{ kN}$ ,  $t=150\text{ s}$ ); (c) Molded patterns in the same condition as in “b” without ultrasonic vibration ( $T_h=180\text{ }^{\circ}\text{C}$ ,  $F=1.0\text{ kN}$ ,  $t=150\text{ s}$ , without ultrasonic vibration); (d) Atmosphere hot embossing ( $T_h=200\text{ }^{\circ}\text{C}$ ,  $F=5.0\text{ kN}$ ,  $t=1,800\text{ s}$ ); (e) Ultrasonic hot embossing by overload ( $T_h=180\text{ }^{\circ}\text{C}$ ,  $F=4.0\text{ kN}$ ,  $t=150\text{ s}$ )

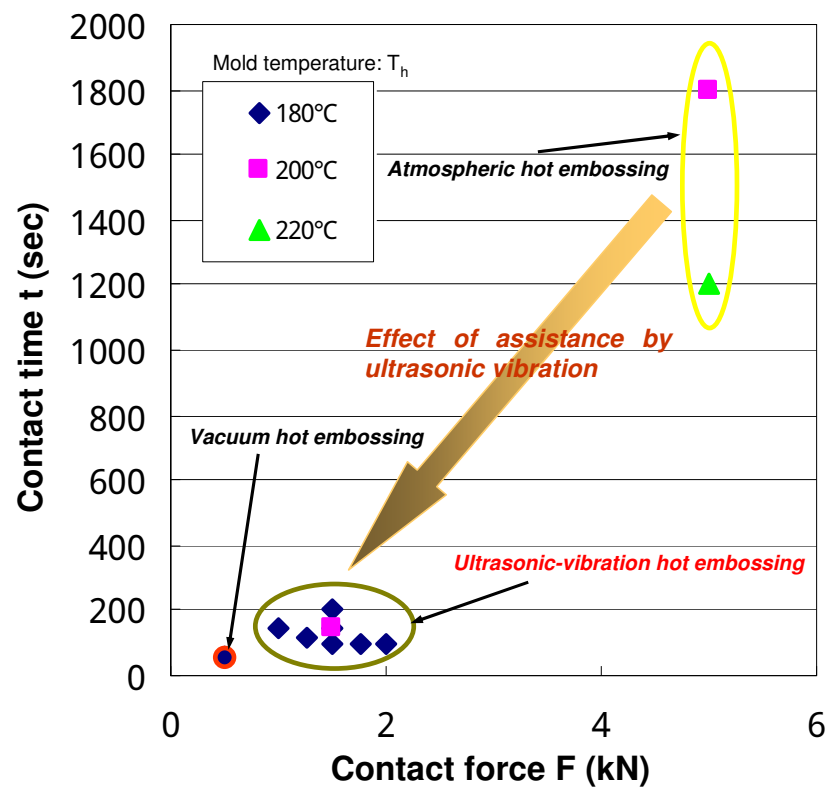


Fig. 5. Effect of assistance by ultrasonic vibration in hot embossing.

and 1/ 12 of their initial values. These results are surprising. It was possible to bring the contact force and time close to the optimum conditions of vacuum hot embossing, although it was molded in the room atmosphere. Thus, it succeeded in molding by combining ultrasonic vibration and hot embossing with a short contact time and a low contact force.

2.2 Incase of impressing ultrasonic vibration with low amplitude

Later, before the author’s new assignment at the National Institute of Advanced Industrial Science and Technology (AIST), another ultrasonic nanoimprint system had also been successful in controlling the flaking from the mold by impressing ultrasonic vibration of the maximum amplitude of 1.8  $\mu\text{m}$  during the de-molding process by a joint development program with Scivax Corporation. The author modified the software of the ultrasonic nanoimprint system where ultrasonic vibration could be applied even to the molding process. By impressing ultrasonic vibration at a maximum amplitude of 1.8  $\mu\text{m}$  the author verified the molding accuracies of patterns ranging in size from 100  $\mu\text{m}^2$  to 1.2  $\text{mm}^2$ . Figure 6 shows a photograph of the ultrasonic nanoimprint system and its cross-sectional view around its loading stages. A metallic mold of a maximum size of 30 mm square was installed in the upper loading stage. A hand-drum-type horn with 1200 W output power and 19 kHz resonance frequency with 1.8  $\mu\text{m}$  maximum amplitude was installed in the upper loading stage of the system where a longitudinal wave of ultrasonic vibration can be generated. Moreover, a ceramic heater and a circulation cooling system with a thermal medium oil were installed between the upper loading stage and the horn. The metallic mold can be heated up to 200 °C. A molding material sheet was held at the bottom loading stage

by a vacuum chuck. The maximum patterning area on the sheet is designed to be 100 x 200 mm<sup>2</sup> by using a step-and-stamp method. The stage has X/ Y translational and  $\theta_z$  rotational capability, and has an alignment accuracy of  $\pm 1 \mu\text{m}$  with 1  $\mu\text{m}$ / pixel image resolution charge-coupled-device (CCD) cameras. Using a cartridge heater, the molding material sheet can be heated up to 150 °C. A contact force up to 4.9 kN can be applied with a servo motor.

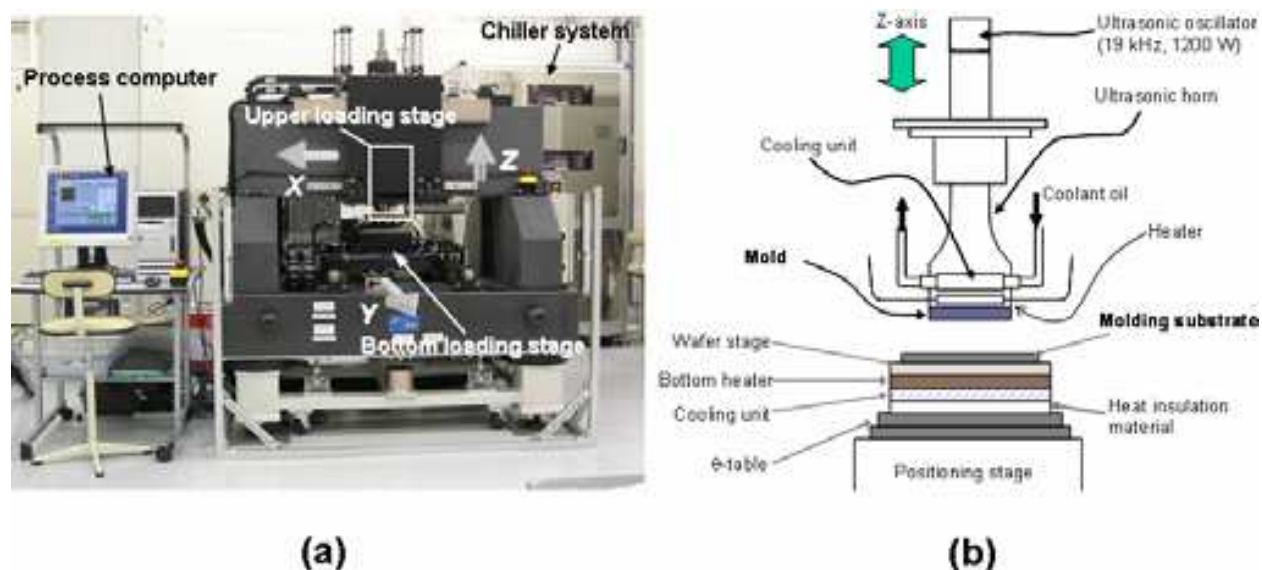


Fig. 6. (a) Photograph of ultrasonic nanoimprint lithography system, and (b) a cross-sectional view of the system around loading stage that includes a piezoelectric actuator.

Based upon the previous experimental result from hot embossing the author chose the heating temperature as 180 °C and varied the contact force from 1.0 to 2.5 kN. Here also, the contact time and the cooling temperature for each setting were kept at 5 min and 130 °C. Figure 7 shows experimental results from each contact force using the same electroformed-Ni mold as shown in Fig. 3. A total of 40 embossed patterns was obtained in one single molding experiment because there were eight impressions for each of the five kinds. The shapes of all these embossed patterns were evaluated by an optical microscope. With this information, the molding rate was calculated for each pattern size. The molding rate was defined as the ratio of the successful pattern to all 8 patterns that were impressed on PC. For instance, when certain size pattern successfully embossed all 8 impressions then the molding rate would be  $8/8 = 1$ . When four impressions successfully embossed then the molding rate would be  $4/8 = 0.5$ . When none embossed, then the molding rate would be  $0/8 = 0$ . For all pattern sizes, the molding rate in the absence of ultrasonic vibration is shown by the left bar chart. When ultrasonic vibration was applied, the molding rate is shown by the adjoining right bar chart. A dramatic change was observed in the molding rate using ultrasonic vibration when the contact force was lowered. In the contact force of 1.0 kN, when ultrasonic vibration was not impressed, the molding rate in pattern size I–V was 0. On the other hand, the molding rate rose up to 0.2 or more when ultrasonic vibration was impressed. As for the molding rate of pattern V, it was found to be low among all contact forces. There are two possible explanations for this. One is that the shape of pattern V was a quadrangular pyramid where the center became a little thinner as shown in Fig. 4. This shape could have been easily damaged during the de-molding process.



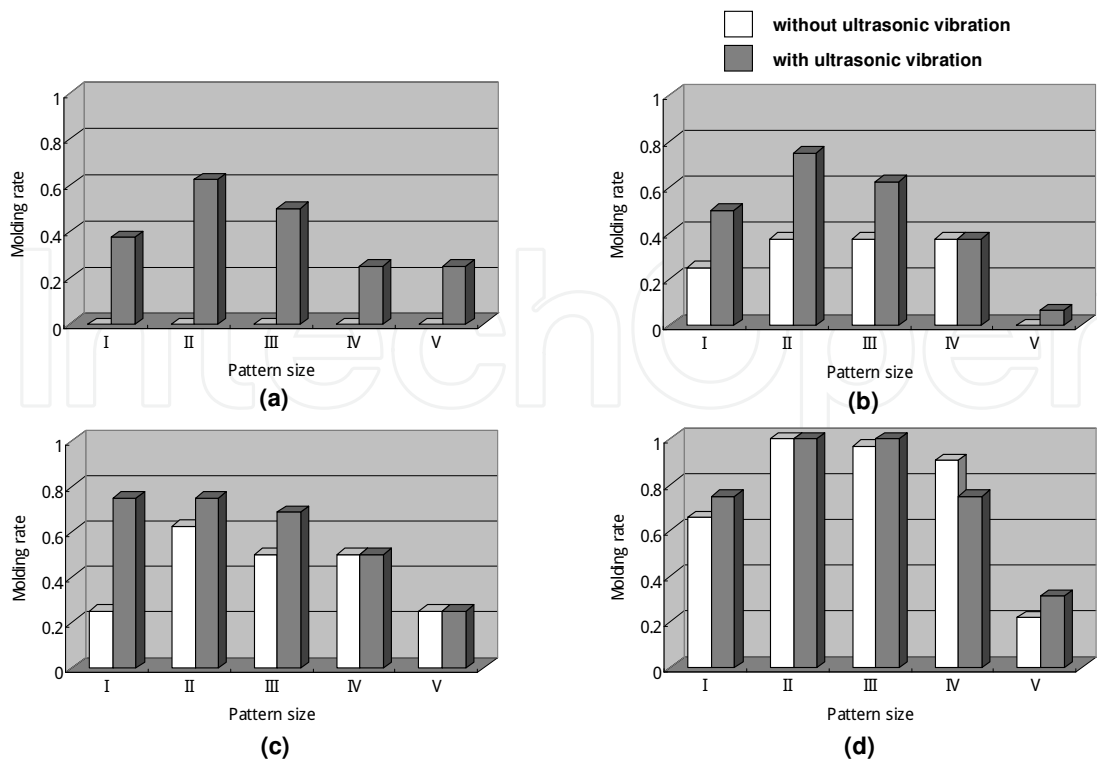


Fig. 7. Relationship between contact force and molding rate. The contact force was: (a) 1.0 kN, (b) 1.5 kN, (c) 2.0 kN and 2.5 kN. The left side shows the usual hot embossing results and the right side shows ultrasonic hot embossing results in the adjoining bar chart. The heating temperature of electroformed-Ni mold, the cooling temperature, the contact time and molding material were 180 °C, 130 °C, 5 min, and PC, respectively.

The other explanation is that the patterns III, IV, and V were located in the central part of the electroformed-Ni mold. For the concave mold, it is necessary to fill the concave pattern by moving the softened molding material from the surroundings of the mold pattern to its central part. Normally, in comparison to the edge of the mold, its center part is not readily molded. Figure 8(a) shows a photograph of an embossed pattern at a contact force of 1.0 kN

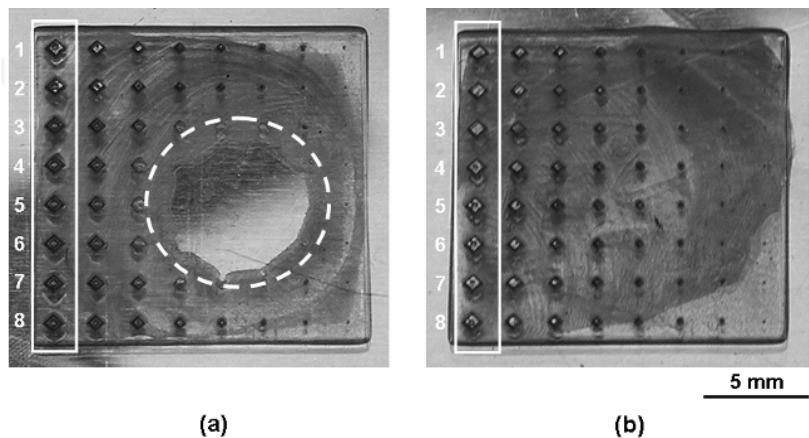


Fig. 8. Photograph of all embossed patterns when the contact force was 1.0 kN: (a) without ultrasonic vibration, and (b) with ultrasonic vibration. An inside of the white dotted circle is a part of flow shortage of PC. White and solid frames are shown as an array of pattern I.

when the ultrasonic vibration was not impressed. It shows that, PC did not reach the center of the mold pattern marked by a white dotted circle. However, by impressing the ultrasonic vibration the PC could be filled to the entire mold pattern as Fig. 8(b). An examination of individual embossed patterns with an optical microscope showed defective molding caused by residual gas where ultrasonic vibration was not impressed. When ultrasonic vibration was impressed, this bubble defect was diminished or completely disappeared. This information led to a great improvement in the molding rate. Optical microscope photographs of the individual embossed patterns from the pattern I are shown in Fig. 9. The impressions 1 through 8 inside the columns defined by the solid white lines in Figs. 8(a) and 8(b) are shown in two rows in Fig. 9. In the top row, the absence of ultrasonic vibration resulted in zero molding rate. Whereas in the bottom row the presence of ultrasonic vibration successfully imprinted patterns No. 1 and 2 with molding rate of 0.25.

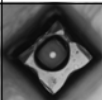
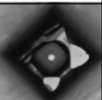
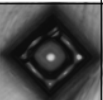
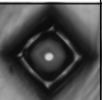
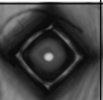
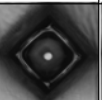
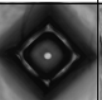
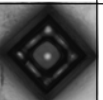
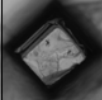
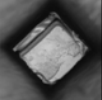
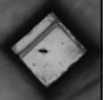
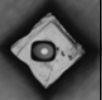
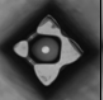
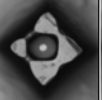
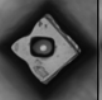
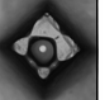
	1	2	3	4	5	6	7	8	Molding rate
Without ultrasonic vibration									0 / 8 = 0
	↓	↓	↓	↓	↓	↓	↓	↓	
With ultrasonic vibration									2 / 8 = 0.25

Fig. 9. Optical micrographs of individual embossed patterns of the pattern I in case of the contact force 1.0 kN.

3. Thermal nanoimprint assisted by ultrasonic vibration

3.1 Step-and-stamp type ultrasonic nanoimprint system

In micropatterning experiments of PC by using the ultrasonic nanoimprint system, the optimized mold heating temperature was 180 °C. As a part of our experiment the above technique was then extended to thermal nanoimprint where the experiment was executed using the same conditions (heating temperature: 180 °C, contact force: 100 N, and contact time: 10 s). The amplitude of ultrasonic vibration could be changed in ten steps (L1 – H5). In nanoimprint experiments a concave Si mold was used where features of its patterns were defined by depth = 3 μm, length = 1.8 μm, and linewidths = 500, 750 nm, and 1 μm. The Si mold was fabricated by micro-electro-mechanical-system (MEMS) processing technologies including an e-beam lithography and a reactive-ion-etching (RIE). The Si mold size was 10 mm square. SEM images of thermal-imprinted patterns with linewidth of 500, 750 nm, and 1 μm at 180 °C are shown in the second row of Fig. 10. The heights of imprinted patterns were measured with a 3D optical profiler NewView 5000 (Zygo Corp.). The PC pattern with a maximum aspect ratio of 5.56 (=2.78 μm/ 500 nm) could be imprinted. However, the thickness of the PC sheet that was originally 0.5 mm had thinned down to 0.27 mm. So as not to consume the PC sheet to much, the mold heating temperature was reduced to 150 °C; this happens to be the almost same as that of the T<sub>g</sub> of PC. The third row in Fig. 10 shows SEM images of imprinted patterns with linewidths of 500, 750 nm, and 1 μm at the heating temperature of 160 °C. A large difference appeared in the molding accuracy when the mold heating temperature was 180 °C. The maximum height of the imprinted pattern was 1.18 μm

in the case where the linewidth was 1  $\mu\text{m}$ , and the highest aspect ratio was 1.06 (= 0.53  $\mu\text{m}$ / 500 nm). In comparison to the case when the mold heating temperature was 180  $^{\circ}\text{C}$ , the highest aspect ratio had decreased to one-fifth of its original value.

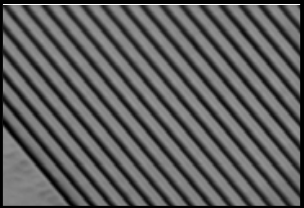
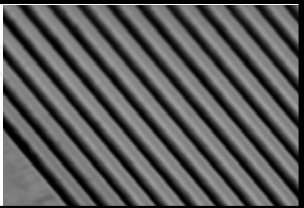
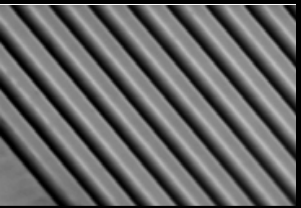
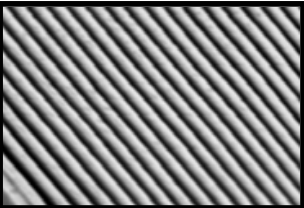
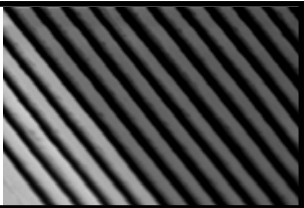
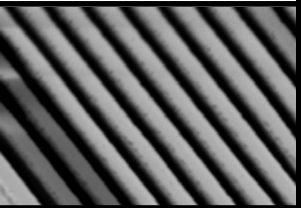
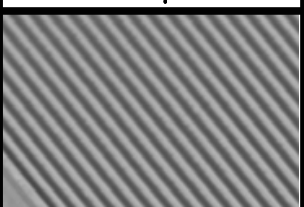
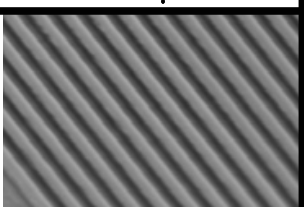
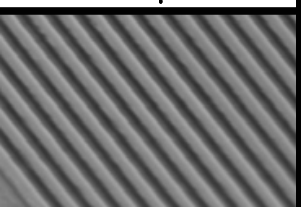
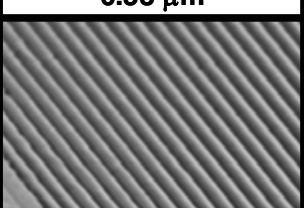
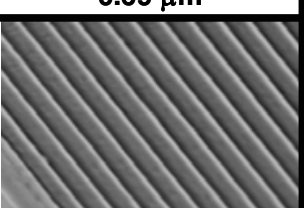
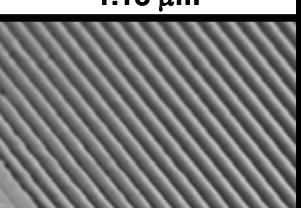
Line width		500 nm	750 nm	1 $\mu\text{m}$
Si mold	SEM image			
	height	2.78 $\mu\text{m}$	2.69 $\mu\text{m}$	3.02 $\mu\text{m}$
PC patterns imprinted at 180 $^{\circ}\text{C}$ without USV	SEM image			
	height	0.53 $\mu\text{m}$	0.69 $\mu\text{m}$	1.18 $\mu\text{m}$
PC patterns imprinted at 160 $^{\circ}\text{C}$ without USV	SEM image			
	height	1.35 $\mu\text{m}$	1.30 $\mu\text{m}$	1.38 $\mu\text{m}$
PC patterns imprinted at 150 $^{\circ}\text{C}$ with 1.8- $\mu\text{m}$ -amplitude USV	SEM image			
	height	0.80 $\mu\text{m}$	0.84 $\mu\text{m}$	1.05 $\mu\text{m}$

Fig. 10. SEM images of nanopatterns in Si mold and PC imprinted by thermal nanoimprint without/ with ultrasonic vibration. “USV” means ultrasonic vibration in the figure.

3.2 Timing of impressing ultrasonic vibration

In the next step, the parameters for ultrasonic nanoimprint were fixed as the following: mold heating temperature = 150  $^{\circ}\text{C}$ , contact force = 100 N, and contact time = 10 s. Figure 11

shows the relationship between the process time and the contact force. The timings I-V in Fig. 11 indicates the starting points of the ultrasonic vibration impression for all ultrasonic vibrations. The first impression marked by I denotes that the timing of ultrasonic vibration began when the contact force was 0 N. In other words, it was the case where the ultrasonic vibration impression began before the Si mold even touched the PC sheet. The markers II, III, IV, and V are the timing points when the ultrasonic vibration impression began after the contact force reached the points 25, 50, 75, and 100 N, respectively. All ultrasonic vibrations were stopped according to the timing VI after being in contact for 10 s. The speed of the press and the release was 1.0  $\mu\text{m/s}$ . Fifty seconds were required from the time Si mold made its initial contact with the PC sheet (contact force = 0 N) to the time when the contact force reached its maximum value of 100 N.

This phenomenon can be clearly confirmed in Fig. 12 (a) where the measurement results of the heights of the imprinted pattern are shown. Especially, the application of ultrasonic vibration according to the early timing seemed to improve the molding accuracy. Heights of the imprinted pattern of all linewidths showed a rise when the impression of ultrasonic vibration began with timings I (contact force = 0 N) and II (contact force = 25 N), as compared with the case where ultrasonic vibration was not applied. Even when the impression of ultrasonic vibration began with other timings, any substantial change was not observed in the pattern with linewidths of 750 nm and 1  $\mu\text{m}$ , though the height of the imprinted pattern with 500 nm linewidth did show a rise. Moreover, when the impression of ultrasonic vibration began on the timing I, the ultrasonic vibration had been continuously impressing for 60 s. Although the contact time was extended to 60 s without applying ultrasonic vibration as shown by the dotted lines in Fig. 11, a noticeable increase in the height of the imprinted pattern was not observed.

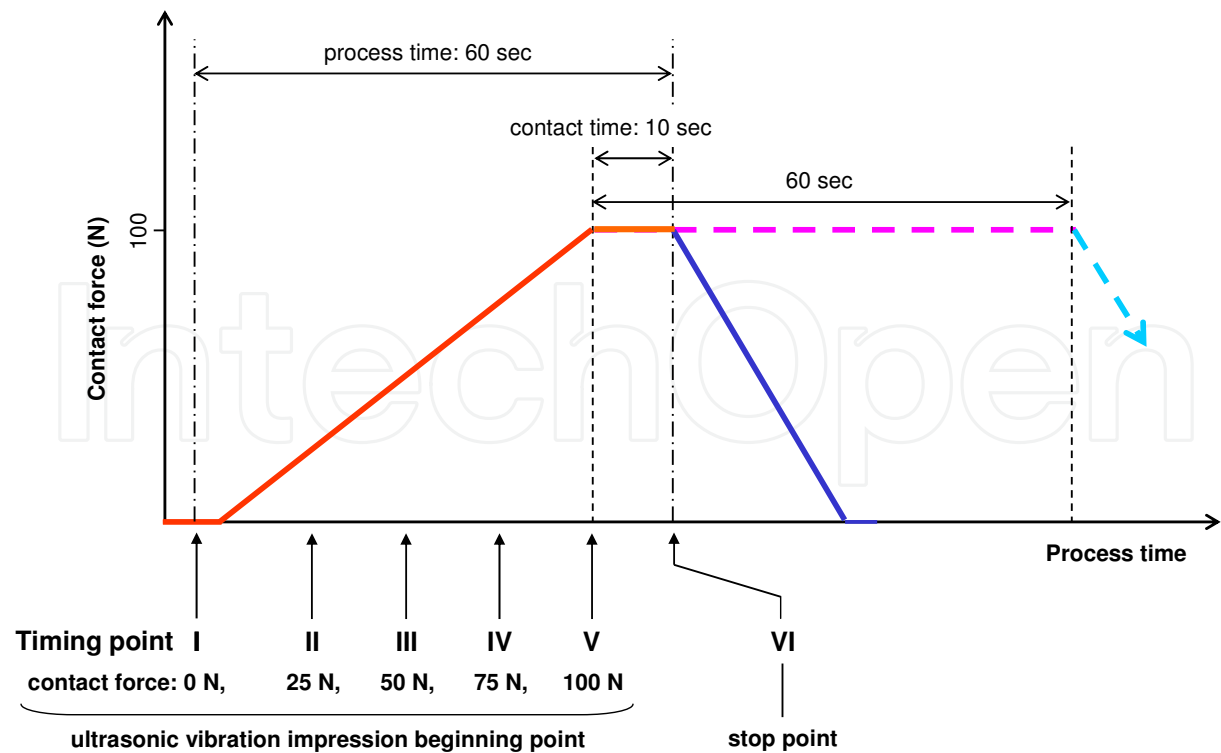


Fig. 11. Relationship between the timing points of applying ultrasonic vibration and contact force.



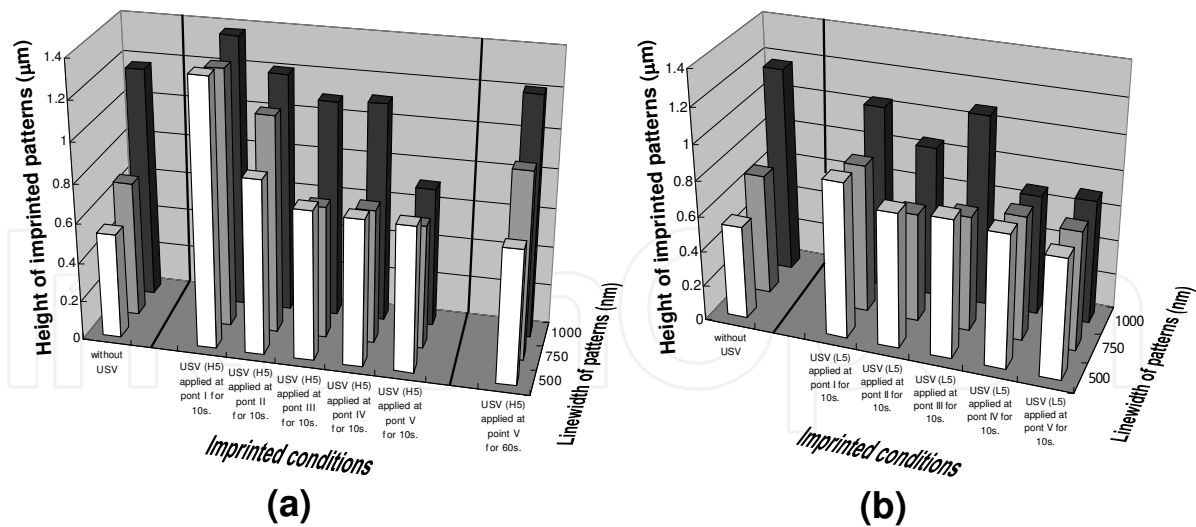


Fig. 12. Height of PC imprinted patterns in ultrasonic nanoimprint: (a) with 1.8-μm amplitude, and (b) with 1.25-μm amplitude. “USV” means ultrasonic vibration in the figure.

When ultrasonic vibration with 1.25 μm maximum amplitude (input voltage level = L5) was initiated at a timing I, the molding accuracy of the imprinted patterns was almost same as in the third row, but was less in comparison to that in the fourth row. This phenomenon can be confirmed by the measurement results of the height of the imprinted pattern shown in Fig. 12(b). No dramatic increase in the height of the imprinted pattern by the difference of timing in which the impression of ultrasonic vibration began could be observed in comparison to the case of the maximum amplitude of 1.8 μm (input voltage level = H5). In the case of the linewidth of 500 nm, the height of patterns with impressing ultrasonic vibration increased in comparison to the case where ultrasonic vibration was not impressed. In the case of the linewidth of 750 nm, it was confirmed that the height of the pattern increased where the impressing of ultrasonic vibration started at the timing I (contact force = 0 N). Such a phenomenon shows that the flowing of the thermoplastic cannot be assisted enough by ultrasonic vibration with low amplitude.

3.3 Decrease in mold heating temperature by assistance of ultrasonic vibration

Typically, the optimal heating temperature in thermal nanoimprint lithography using PC is 180 °C, but when ultrasonic vibration is applied, it becomes possible to mold nanopatterns at a lower temperature. As a result, the process time of a thermal cycle could be cut into half; thus improving the throughput greatly. In this experiment, a convex Si mold was fabricated by MEMS processing technologies as shown in Fig. 13. The pattern includes 36 cross-marks, and each cross-mark exists inside of a 500-μm<sup>2</sup> square frame. The shape of the cross-mark is in the form of a cross where two rectangles (400 x 10 μm<sup>2</sup>) cross each other. Four crossmarks, enclosed in a frame of white dotted lines in Fig. 12(a), were designed as alignment markers for step-and-stamp nanoimprinting.

In the alignment process, an image of the crossmarks is captured by a 1 μm/ pixel CCD camera and is then used by the computer to automatically adjust the position of the stage. The cross-mark was composed of a nanopattern whose size was below the resolution of the CCD camera. Therefore, the entire cross-mark appeared fuzzy, and darker than its surrounding. Figure 13(b) shows the arrangement of figures inside the frame of the dotted



white dotted lines in Fig. 13(a). These cross-marks arranged in the frame were composed of four types of nanopatterns. The nanopatterns on the upper left, upper right, lower left, and lower right were labeled as A, B, C, and D, respectively. Pattern A was a line and space pattern with 750 nm linewidth and 1.5  $\mu\text{m}$  pitch, pattern B was a line and space pattern with a 500 nm linewidth and 1  $\mu\text{m}$  pitch, pattern C was a dot pattern of 750 nm<sup>2</sup>, and pattern D was a dot pattern of 500 nm<sup>2</sup>.

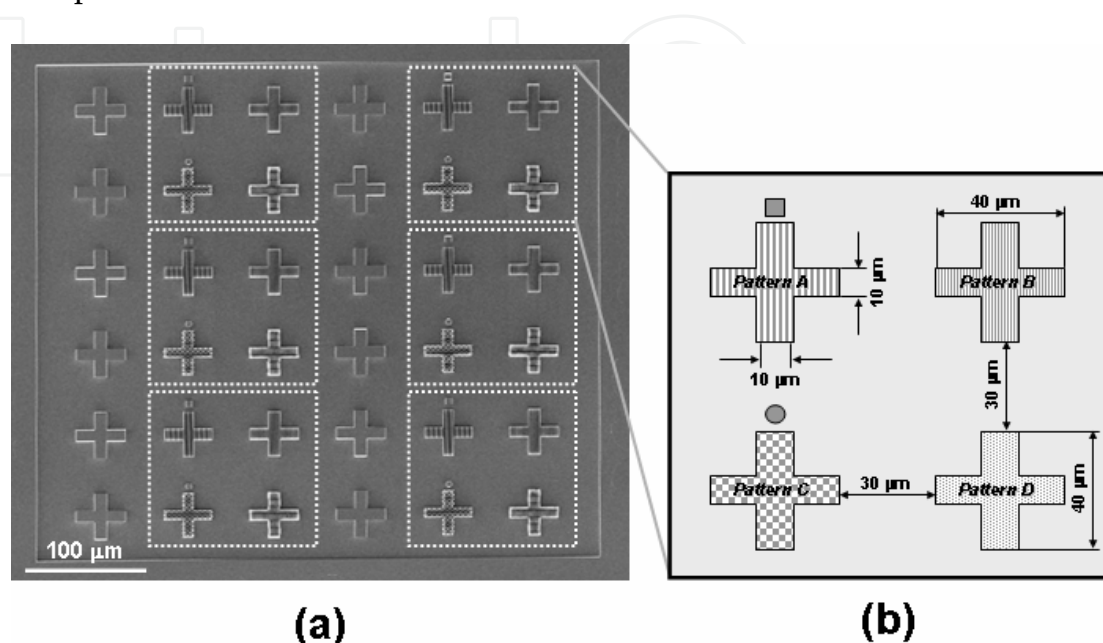


Fig. 13. (a) SEM image of Si mold pattern, and (b) schematic of cross-marks in white square from the left figure.

In the previous work, the molding conditions that could shorten the process time of one cycle in thermal nanoimprint were investigated. As a result, it was possible to imprint in a shorter period of time when the heating temperature, contact force, contact time, cooling temperature and molding and de-molding speeds were 180 °C, 100 N, 10 s, 130 °C and 1.0  $\mu\text{m/s}$ , respectively. After the contact force reached 100 N, the contact force was kept during 10 s and then the cooling process was started. Figure 14(a) shows an optical microscopy photograph of the PC pattern imprinted under these conditions.

The shape of the imprinted pattern was primarily evaluated by optical microscopy considering the fact that in actual alignment it is the optical image that the CCD camera looks at. The cross-marks composed of the four types of nanopatterns can be clearly seen in Fig. 14(a). On the other hand, for the cross-mark with no nanopattern, only the edge part appeared to be somewhat blackish. Next, the cooling temperature, contact force, and contact time were fixed at 130 °C, 100 N, and 10 s, and thermal nanoimprint was carried out with the heating temperatures of the Si mold set at three different low values, i.e., 170, 165, and 160 °C. Optical microscopy photographs of each PC pattern when the heating temperatures were 170, 165, and 160 °C are shown in Figs. 14(b)–14(d), respectively. Similar images were observed for the pattern molded with the heating temperatures of 180 and 170 °C. The contrast between the PC pattern and the surrounding became less pronounced at a heating temperature of 165 °C. When the heating temperature was 160 °C, the cross-mark composed of the nanopattern could not be resolved.

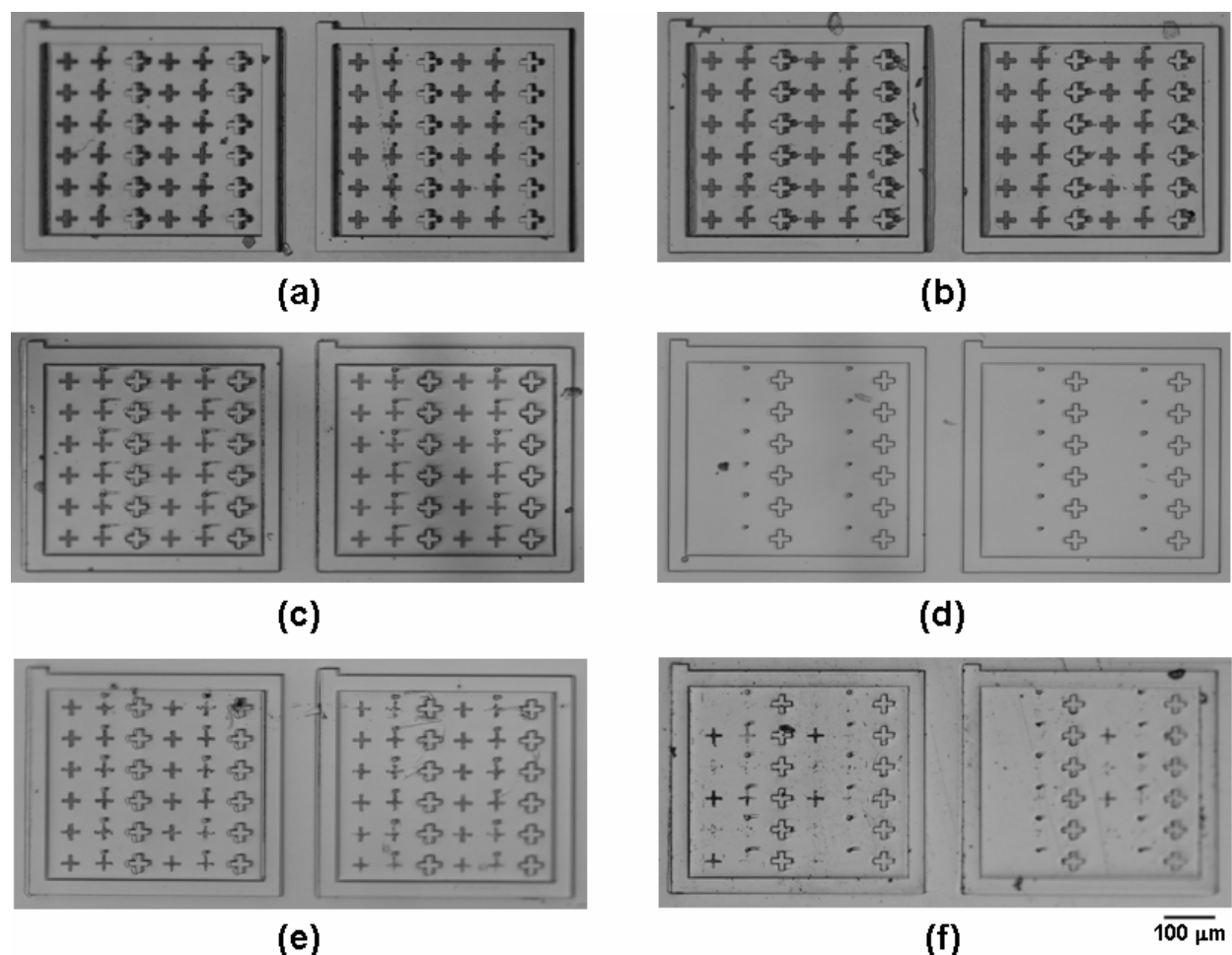


Fig. 14. Optical micrographs of PC imprinted patterns using thermal nanoimprint without ultrasonic vibration. The heating temperatures were: (a) 180, (b) 170, (c) 165, and (d) 160 °C. Optical micrographs of PC imprinted patterns using thermal nanoimprint with ultrasonic vibration. Ultrasonic vibration impression was started when the contact force reached to (e) 20 N and (f) 100N. The contact force and contact time were 100 N and 10 s, respectively.

In the next experiment, the contact time and contact force were 10 s and 100 N, and ultrasonic vibration with a maximum amplitude of 1.8  $\mu\text{m}$  was simultaneously impressed during the contact time. Figures 14(e) and 14(f) show an optical microscopy photograph of the PC pattern from a separate experiment in which ultrasonic vibration impression began when the contact force reached 20, and 100 N, respectively. All the cross-mark images can be confirmed in Fig. 14(e). The contrast of the pattern and the circumference part becomes overwhelmingly clear when compared with the experimental result of thermal nanoimprint at 160 °C. Some cross-marks can be observed in Fig. 14(f). The cross-mark composed of the dotted pattern of 750 nm squares could be observed with high contrast. It turned out that nanoimprint became feasible by impressing ultrasonic vibration below the molding boundary condition of thermal nanoimprint. In addition, it was confirmed that the timing of the initiation of the ultrasonic vibration impression played an important part here, and that the use of ultrasonic vibration was an effective way to nanoimprint. And moreover, the molding accuracy improved even further when a contact force was applied.

## 4. Ultrasonic nanoimprint

### 4.1 Exchange of a piezoelectric actuator to magnetostriction actuator in ultrasonic nanoimprint system

The step-and-stamp type ultrasonic nanoimprint system was originally designed and built so that ultrasonic vibration could be impressed in the de-molding process. However, the available power for ultrasonic vibration was insufficient hence the author substituted magnetostriction actuator for piezoelectric actuator in the ultrasonic generator that provided relatively high amplitude. This led to the development of ultrasonic nanoimprint technology capable of imprinting from mold at room temperature that required neither heating nor UV radiation.

An assembly drawing and a photograph around the loading stages of the ultrasonic nanoimprint system are shown in Figs 15(a) and 15(b). Loading stages are composed of an upper loading stage that fixes a mold and a bottom loading stage that fixes a molding material. A parallel adjustment mechanism using spherical sliding was connected to the upper loading stage. A magnetostriction actuator AU-010N300-MS1 (ETREMA Product Inc.) was built into the upper loading stage, and the longitudinal wave of ultrasonic vibration with the frequencies of DC - 20 kHz and the amplitudes of 0 - 5  $\mu\text{m}$  can be generated.

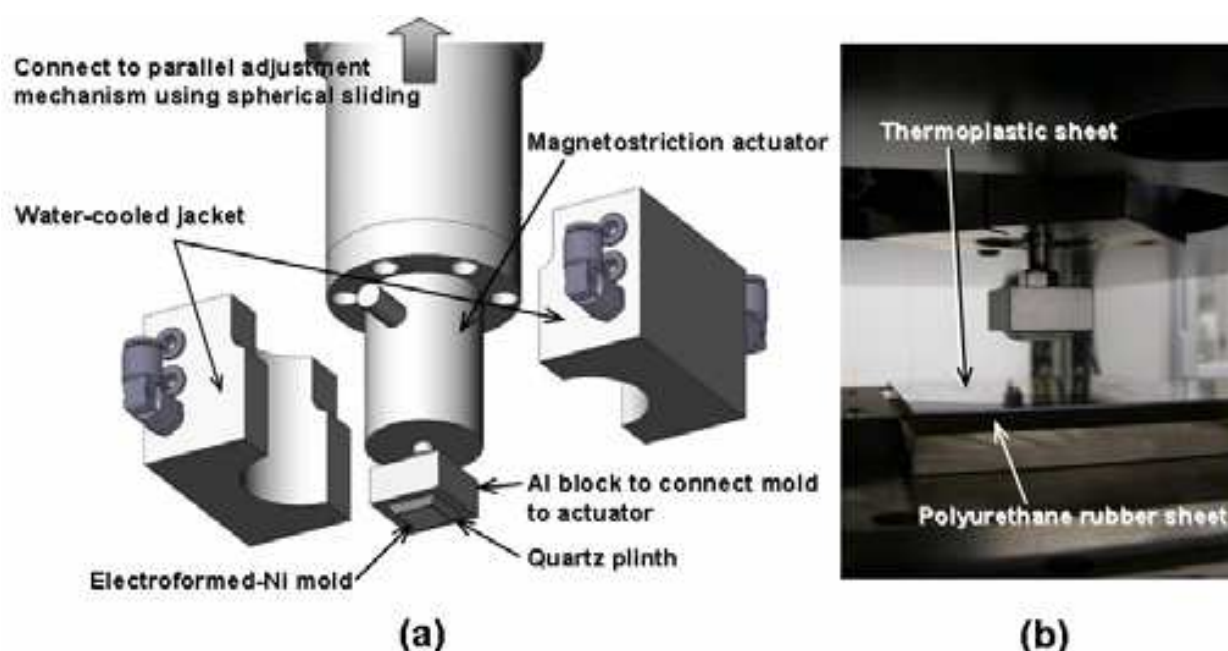


Fig. 15. (a) Assembly drawing of the upper loading stage, and (b) photograph of the upper and bottom loading stages in an ultrasonic nanoimprint system.

The magnetostriction actuator generates heat during its operation. To protect the magnetostriction actuator from heating and to prevent the heat from propagating into the other parts of the mold, the magnetostriction actuator was covered by a water-cooled jacket to cool it down to 20 °C. An Al block with a surface area of 30 mm<sup>2</sup> was fixed on the head of the magnetostriction actuator. The relationship between the frequency and amplitude of ultrasonic vibration had been investigated before the imprint experiments. The amplitude of ultrasonic vibration increased up to 10  $\mu\text{m}$  for the resonance frequency of 8 kHz. At frequencies above 10 kHz the magnetostriction actuator hardly could oscillate. Then by

adjusting the input current within a frequency range of DC - 10 kHz it was improved where it could run continuously with an amplitude of 3  $\mu\text{m}$ . When the input current rose up to 4 A, the oscillation of the ultrasonic vibration stopped; it was caused by an overload at the frequency 10 kHz. A mold was bonded on the Al block with a negative-tone UV resist PAK-01 (Toyo Gosei Co., Ltd.) through a quartz plinth. The ditch for a vacuum chuck was processed on the surface of the bottom loading stage, and the molding material of a thickness 0.5 mm was fixed through an elastic material of 3 mm thickness. Clear-through-holes were processed at the same locations as in the ditch of the vacuum chuck in the elastic material.

Figure 16 shows a 15 x 15 mm<sup>2</sup> electroformed-Ni mold (Scivax Corp.) used for this experiment. As for the mold pattern, a basic unit of 2 mm<sup>2</sup> shown in the right half of Fig. 16 was arranged in a 5 x 5 matrix. Convex line/ space (L/ S) patterns and convex/ concave circle dot patterns were put into this basic unit. There are eight sizes of patterns between 0.5 and 10  $\mu\text{m}$ , with pattern height/ depth being 1  $\mu\text{m}$ . To ease the release of the mold, a self-assembled monolayer (SAM) of a release agent was formed on the surface of the electroformed-Ni mold. For this purpose, Optool HD-2101TH (Daikin Industries Ltd.) was spread on the electroformed-Ni mold by a nanoimcoater NIC-0703 type N (Eintesla, Inc.), followed by a 30 min of drying that established a SAM on the surface of the mold material.

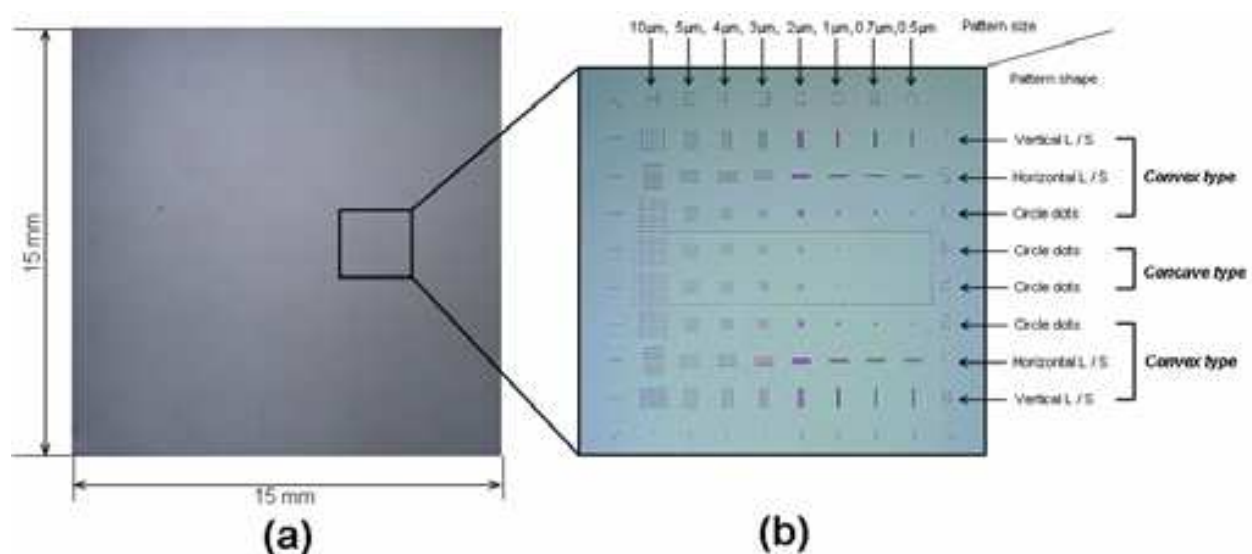


Fig. 16. Photographs of electroformed-Ni mold and mold patterns.

#### 4.2 Optimization of molding conditions for PET in ultrasonic nanoimprint

The molding material selected was polyethylene terephthalate (PET,  $T_g = 75\text{ }^{\circ}\text{C}$ ) because among the engineering plastics its  $T_g$  is comparatively low. The PET sheet was 100 mm square in area and 0.5 mm in thickness. As a preliminary experiment in nanoimprinting, the imprinted pattern depth was investigated under conditions where pressure was applied, but no ultrasonic vibration was involved. The depth of the pattern was measured using a five-line confocal microscope Optekics S130 (Lasertec Corp.). The result of this experiment is shown in Figs. 17(a) – 17(c). It was possible to imprint on PET using only the contact force if the imprinted pattern depth were less than 0.5  $\mu\text{m}$ . When the contact force was set at 50, 100, 250, 500, 750, or 1000 N, the expectation that the imprinted pattern depth would increase slightly with increasing force turned out to be the case only where the pattern width was 1



$\mu\text{m}$  or less. Moreover, in the experiment the contact time was also varied and was set to 10, 20, 30, 60, or 90 s. The imprinted pattern depth became deeper accordingly with the contact force when the contact force was 50 and 100 N. However, when the contact force became 250 N or more, any further variation in contact time showed no effect on the pattern depth. The contact force might cause a shift from elastic deformation to plastic deformation between 100 and 250 N on the surface of PET, although it is considerably lower than the compressive strength of bulk PET (110 - 123 MPa). The next experiment addresses the depth of the imprinted pattern when ultrasonic vibration was also applied, while using the same imprint conditions as in the previous case. The results are shown in Figs. 17(d)-17(f). It is now well understood that applying ultrasonic vibration overall deepens the imprinted pattern further. In general, it has also been confirmed that if the contact time became long, the imprinted pattern depth would become deeper. More frictional heat develops when the impressed time of ultrasonic vibration is prolonged. The molding accuracy seemed to improve in ultrasonic nanoimprint because the transformation by contact force was combined with the softening of the plastic by frictional heat. However, the best conditions for the contact force depend on the width of the pattern. The optimized contact force, when the width of the pattern was 500 and 700 nm, was 250 N; and when the width of the pattern was 1  $\mu\text{m}$ , the optimized force was 500 N. Specifically, it succeeded in complete transcriptions of the 1- $\mu\text{m}$ -wide imprinted pattern to a depth of 1  $\mu\text{m}$ , where the optimized conditions were a contact force of 500 N and a contact time of 60 s. We believe that, because ultrasonic vibration was held down while the contact force was growing too much, the effect of the assistance of ultrasonic vibration was impeded.

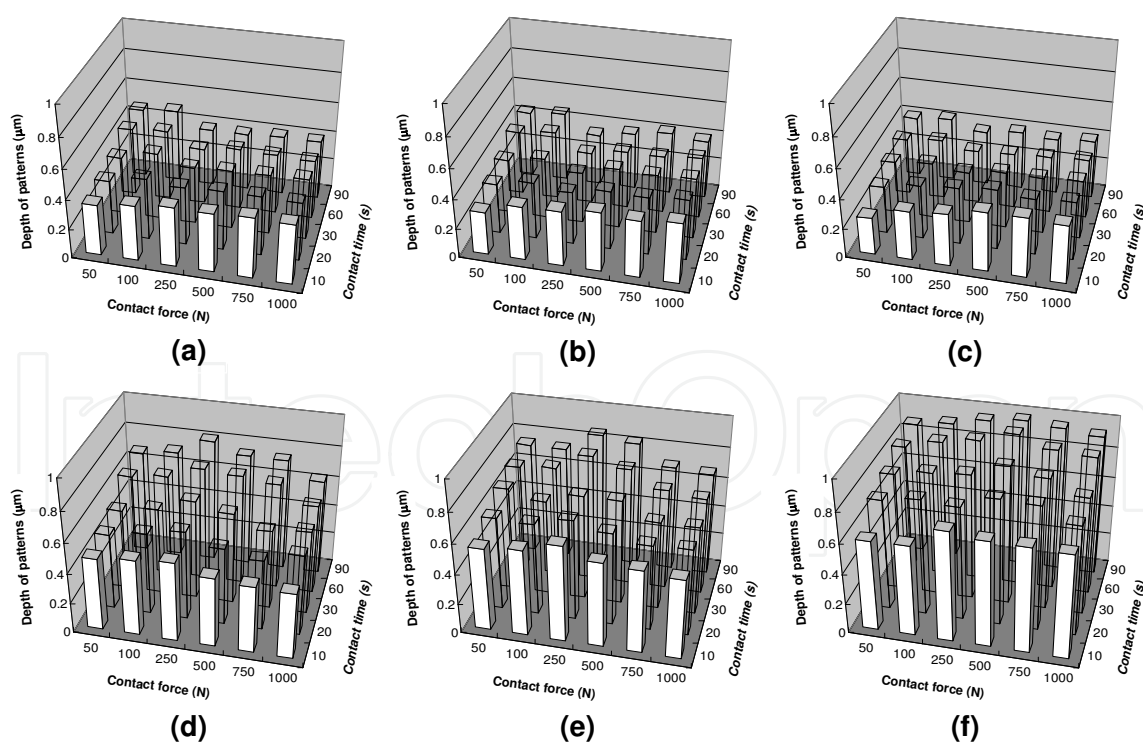


Fig. 17. Relationship between contact force or contact time and imprinted pattern depth without ultrasonic vibration for linewidths of (a) 500 nm, (b) 700 nm, and (c) 1  $\mu\text{m}$ . Relationship between contact force or contact time and imprinted pattern depth in ultrasonic nanoimprint for linewidths of (e) 500 nm, (f) 700 nm, and (g) 1  $\mu\text{m}$ .



In the next step, the author investigated the frequency/ amplitude of ultrasonic vibration dependency of the molding accuracy in the ultrasonic nanoimprint by the magnetostriction actuator with a changeable frequency. Because displacement of the magnetostriction material is larger than the piezoelectric materials, the magnetostriction actuator doesn't need a resonance horn like the piezoelectric actuator. Therefore, the magnetostriction actuator can change the frequency of ultrasonic vibration. Then, a bipolar DC power supply BP4610 (NF Corp.) was connected with the magnetostriction actuator. When the frequency was increased from 0 to 10 kHz in five steps the depths of the imprinted patterns also became deeper, regardless of their linewidths. Especially at the frequencies of 5 kHz and higher, the imprinted depths increased at a greater rate as shown in Fig. 18(a). Next, while keeping the frequency fixed at 10 kHz, the amplitude was increased from 0 to 4  $\mu\text{m}$  in nine steps as shown in Fig. 18(b). The figure shows the relationship between the depth of the imprinted pattern and the amplitude of the ultrasonic vibration. The depths of the imprinted patterns became deeper with increasing amplitudes regardless of patterns' linewidths. A 1- $\mu\text{m}$ -width pattern was imprinted fully when the amplitude was 3  $\mu\text{m}$ .

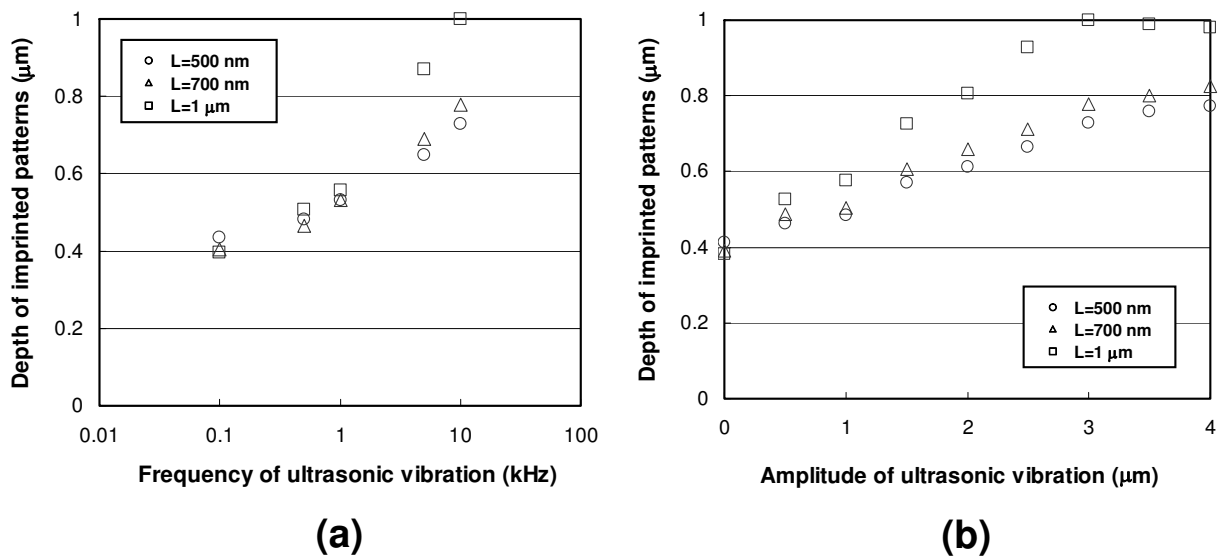


Fig. 18. (a) Relationship between frequency of ultrasonic vibration and depth of imprinted pattern with different pattern widths in ultrasonic nanoimprint, and (b) relationship between amplitude of ultrasonic vibration and depth of imprinted pattern with different pattern widths in ultrasonic nanoimprint.

4.3 Ultrasonic nanoimprint on engineering plastics

Before applying the optimized imprint conditions for PET to other engineering plastics, the author investigated the  $T_g$  and the hardness of various engineering plastics and examined them as an index for comparison. There are five kinds of engineering plastics; those, besides PET, are acrylonitrile butadiene styrene (ABS) resin, polymethyl methacrylate (PMMA), cyclo olefine polymer (COP), polycarbonate (PC), and polyimide (PI) as shown in Table 1. Figure 19 shows optical photomicrographs of the center unit in the imprinted pattern. In all engineering plastics, a concave mold pattern which reverses to a convex imprinted pattern, could not be transferred. However, the transfer of a convex mold pattern, which reverses to a concave imprinted pattern, could be confirmed, although there was a difference in the

Materials	PET	ABS	PMMA	COP	PC	PI
Glass transition temperature (°C)	69	105	114	138	144	336
Indented depth (nm) when loading force was 10 mN	2342	2603	1656	4731	1891	1598

Table 1.Estimated  $T_g$  and measured indented depths of PET, ABS, PMMA, COP, PC, and PI. contrast. In convex patterns the structure that bulges from the mold surface pushes the molding material to the outside of the pattern region. In concave patterns, it is necessary to draw the molding material from the outside of the pattern region toward the inside of the region to fill in the cavities with the molding material. When imprinting where the ambient is room atmosphere, it is difficult to imprint with the concave patterns because the air trapped inside the cavity is likely to cause distortion of the fillings of the molding material. Therefore, a convex pattern generally can be easily imprinted in comparison to that of concave patterns. The vertical stripes on the surface of ABS and PI, as shown in Figs. 19 (b) and 19(f), are caused during the operation when the sheets are polished down to a thickness of 0.5 mm by the plastic supplier.

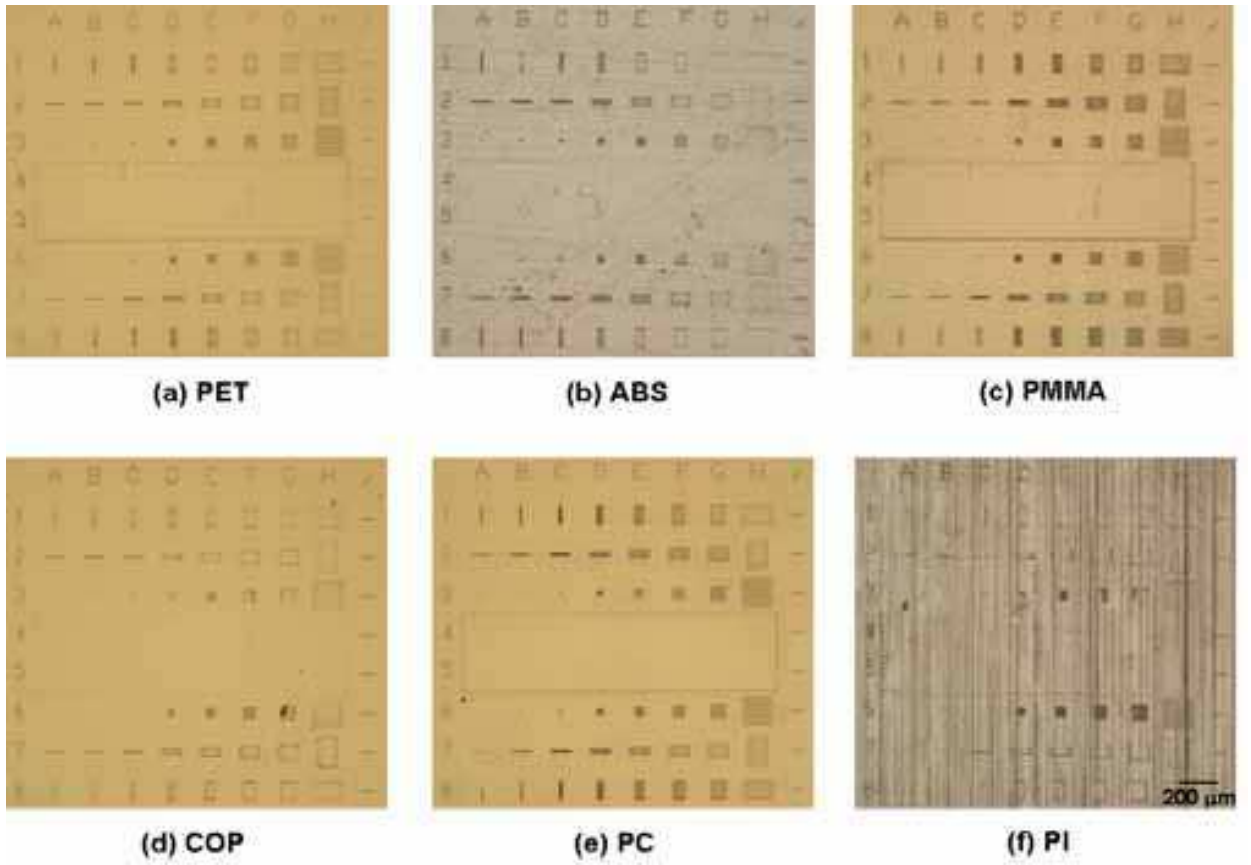


Fig. 19. Optical micrographs of imprinted patterns on (a) PET, (b) ABS, (c) PMMA, (d) COP, (e) PC, and (f) PI.

After observation by an optical microscope, a 20-nm-thick film of Au was sputter deposited on the surface of the imprinted pattern. The result of observing L/ S patterns with the


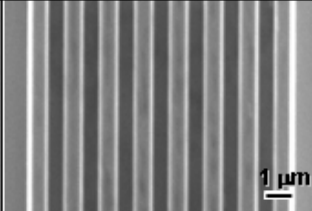
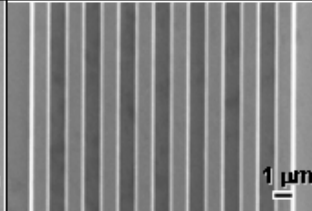
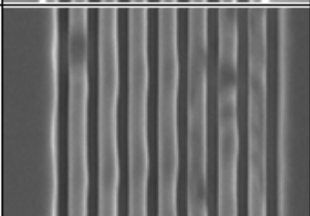
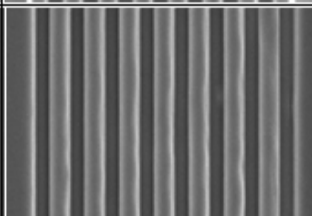

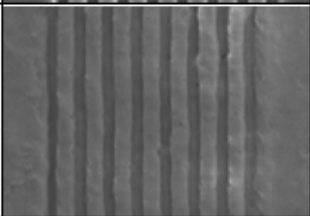
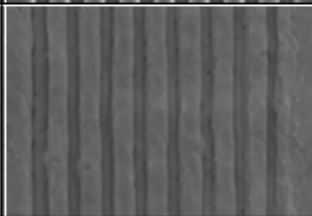

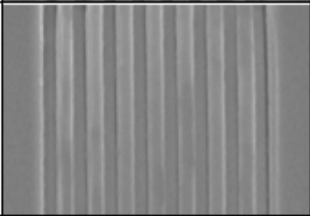
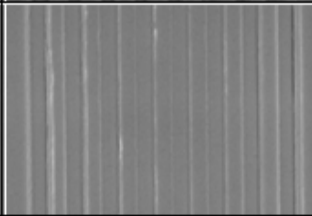
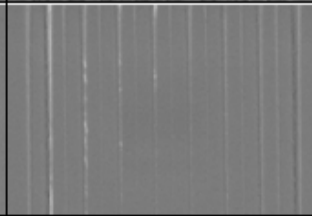
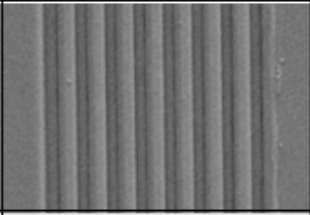
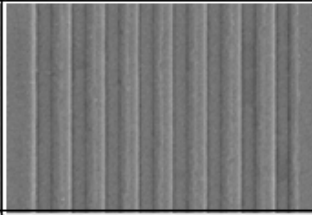
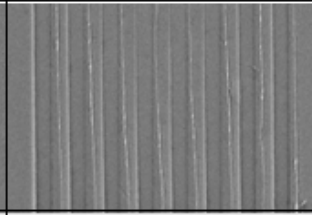
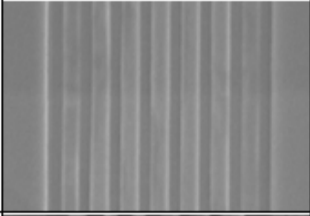
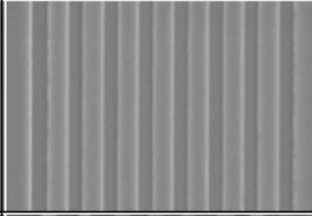
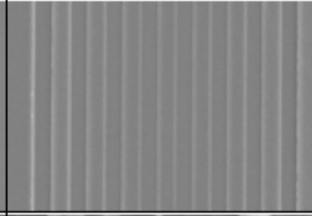
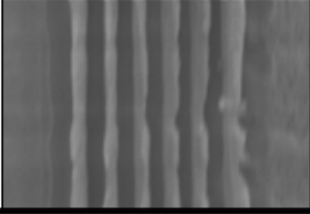
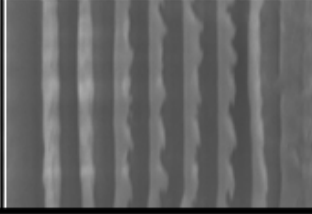
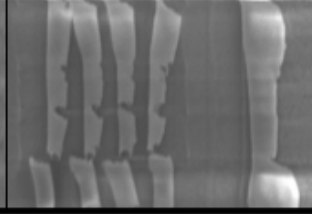
Line width	500 nm	700 nm	1 μm	Ra
Ni mold				5 nm
PET				5 nm
ABS				20 nm
PMMA				2 nm
COP				17 nm
PC				5 nm
PI				15 nm

Fig. 20. SEM images and average surface roughness of L/ S patterns imprinted on PET, ABS, PMMA, COP, PC, and PI.

linewidths of 500 nm, 700 nm, and 1 μm by SEM is shown in Fig. 20. The upper line in Fig. 20 shows mold patterns of the electroformed-Ni mold. In the SEM observation, we checked

the shape of the edge and the surface roughness of the imprinted pattern. The average surface-roughness ( $R_a$ ) of 1- $\mu\text{m}$ -width imprinted patterns was measured by the 3-D optical profiler as shown in Fig. 20. In PET, the edge is sharp and the surface is also smooth. In the imprinted pattern with the linewidth of 500 nm, the part where the contrast was weak, was observed for the incomplete filling. In the imprinted pattern of all linewidths on ABS, the edge became rounded, and the shape of the melted plastic solidified within a short time without relaxing. In PMMA, although the edge of the imprinted pattern was sharp, the surface was very smooth. In the imprinted pattern on COP, the edge became duller, and the surface was rough. In PC, the sharpness in the edge was that of the middle of PMMA and COP, and the surface was as smooth as that of PET. The imprinted pattern on PI was quite different from that of the other engineering plastics. A phenomenon where a surface layer rolled up from the PI substrate was observed.

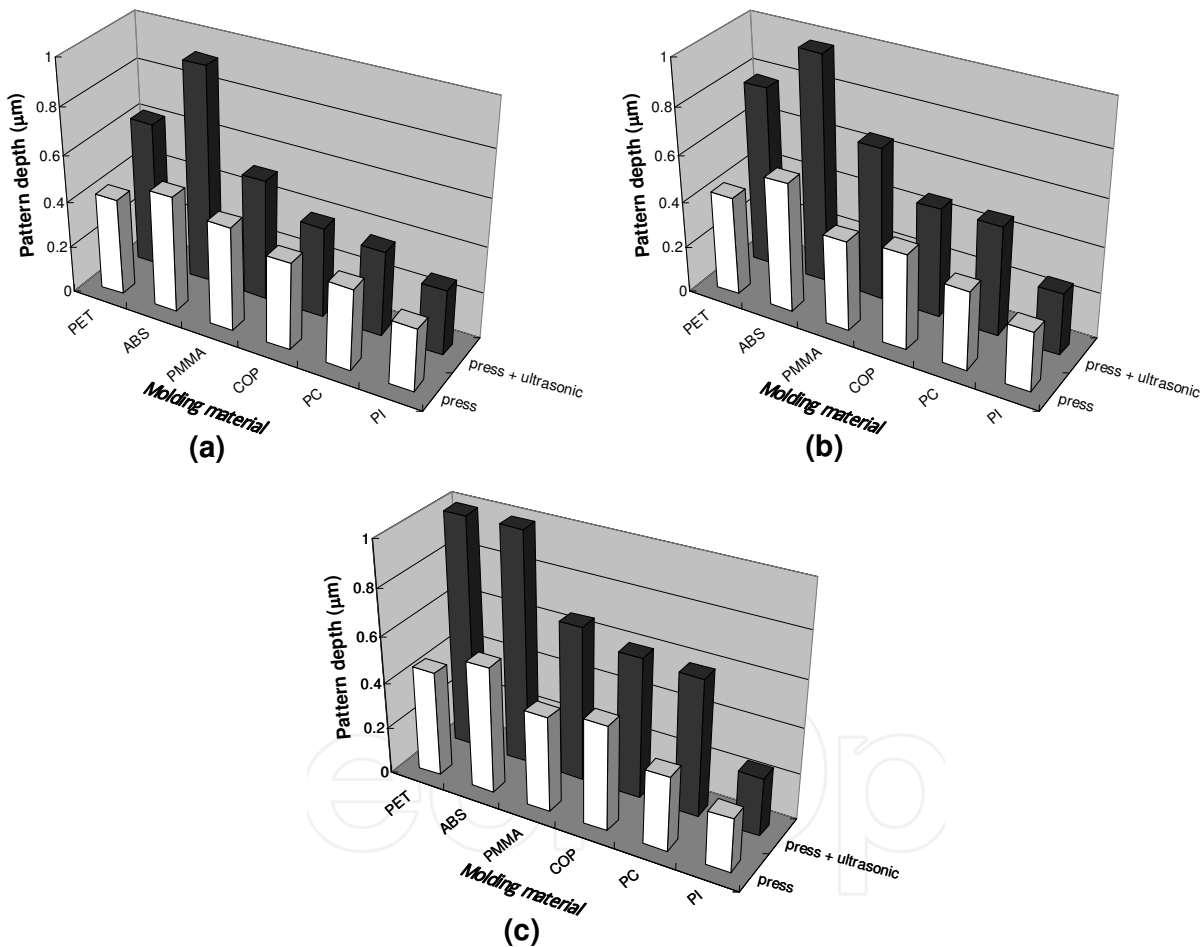


Fig. 21. Relationship between  $T_g$  of engineering plastics and depth of imprinted pattern in widths of (a) 500 nm, (b) 700 nm, and (c) 1  $\mu\text{m}$ .

The depths of these imprinted patterns in the widths of 500 nm, 700 nm, and 1  $\mu\text{m}$  were measured using the confocal microscope, and the data are shown in bar chart form in Fig. 21 arranged from the material with lowest  $T_g$ . Even where ultrasonic vibration was not applied, the mold pattern was transferred by the plastic deformation. In PET, ABS, and COP, the pattern was imprinted comparatively. The result concerning these materials corresponds to

the fact that the maximum depth was largest in Table 1. On the other hand, lower  $T_g$  of an engineering plastic resulted in deeper patterns when ultrasonic vibration was applied. In all engineering plastics, the mold pattern was imprinted quite deep when the pattern width became large. This feature was clearly observed in PET and it succeeded to imprint 1  $\mu\text{m}$  pattern depths in PET and ABS. The difference between the depths of the imprinted pattern from the cases where the ultrasonic vibrations were “applied” and “not applied” seemed to diminish with the rise in  $T_g$ . Especially, there was hardly any difference in depth of the imprinted pattern on PI with the  $T_g$  of more than 300 °C. Black histograms show the depths where the initial plastic deformation was accompanied by thermal deformation of ultrasonic nanoimprint. The difference between these white and black histograms becomes significant in comparison to the cases of materials with high  $T_g$  values. Naturally, it is easier to deform thermally an engineering plastic with low  $T_g$  values. ABS was processed to a maximum depth at an initial pressure, and it was also processed to a maximum depth in the case of ultrasonic nanoimprint. Therefore, it is concluded that impressing the ultrasonic vibration also deforms the pattern thermally after the pattern has already undergone its initial plastic deformation. In the ultrasonic nanoimprint, the molding material seemed to imprint quite deep by thermal deformation generated by the frictional heat after the transformed plasticity by the contact force in the initial process.

#### 4.4 Ultrasonic nanoimprint on spin-on-glass (SOG)

The ultrasonic nanoimprint technology was also employed for patterning on the spin-on-glass (SOG) coated substrate. Accuglass 512B (Honeywell Co., Ltd.), an organic SOG and known as methyl siloxane was used for experiments on ultrasonic nanoimprint. The chemical formulae of Accuglass 512B is  $\text{CH}_3\text{Si}_2\text{O}_{3.5}$ , with 14 % content of carbon. A 400- $\mu\text{m}$ -thick and 100-mm-diameter Si wafer was prepared by polishing both its sides by CMP (chemical-mechanical-*polishing*). A 10-nm-thick Ti layer was sputter-deposited as an interlayer to improve the adhesion between the SOG layer and the Si substrate. In general, SOGs require a two-step thermal-treatment that involves baking at low, and then at a high temperature. We baked the SOG/ Ti/ Si substrate at 150 °C for 10 s using a hot plate as a 1st annealing after SOG spin-coating. The substrate was then allowed to naturally cool down to room temperature, and then was heated up to 450 °C by a rapid thermal processor AS-One 100 (Annealsys) for 1 h as its 2nd annealing. And then the ultrasonic nanoimprints was verified on the SOG coated substrates. Molding conditions and an electroformed-Ni mold were the same as in the case of the ultrasonic nanoimprint experiments on engineering plastics in the above paragraph. Figure 22 shows the result of transferring line/ space patterns with the linewidths of 500 nm, 700 nm, and 1  $\mu\text{m}$  on SOG coated Ti/ Si substrates under these conditions. We succeeded in ultrasonic nanoimprinting on all substrates regardless of the linewidths of the mold pattern. Though the edges were relatively sharp, fine structures like detailed cracks could be observed on the bottom surface of the line/ space patterns in the SOG/ Ti/ Si substrate after the 1st annealing. On the other hand, the edge was very shaggy, although the bottom surface of the imprinted pattern was relatively smooth in SOG/ Ti/ Si substrate that was annealed at 450 °C for 1 h. The surface of the SOG layer before hard baking was damaged, and the part where mold patterns came into contact was rubbed and crushed by ultrasonic vibration. When the molding material is thermoplastics, the temperature of the molding material locally seems to rise to close to the  $T_g$  of thermoplastics because of the frictional heat generated by ultrasonic vibration.



Therefore, the bottom surface of concave imprinted patterns, crushed by mold patterns, solidified to a relatively smooth surface after being softened by ultrasonic vibration. However, because our ultrasonic nanoimprint system did not have power strong enough where the annealed SOG could be softened again, the surface of the crushed SOG layer remained rough. On the other hand, a burr appeared in the imprinted pattern like the ones seen in metal structures when cut with a tool bit or milled with an endmill, because the surface of SOG after hard baking had become relatively hard. SOG in the part where mold patterns came in contact was flattened, and grinding swarms of SOG that were pushed away from the center were piled up as a burr on the sidewall of the imprinted pattern. Thus, the processing principle of ultrasonic nanoimprint on SOG seemed to be quite different in the cases of before, and after hard baking. Even if each SOG coated substrate were imprinted without applying ultrasonic vibration under the same contact force and contact time, imprinted patterns could not have been observed.

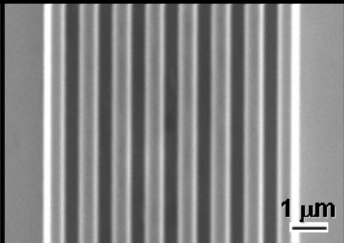
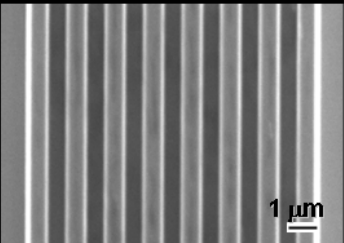
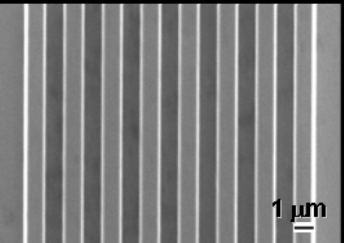
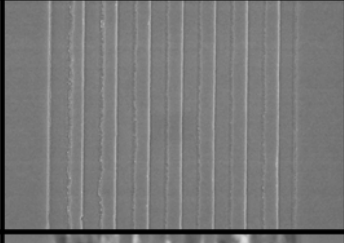
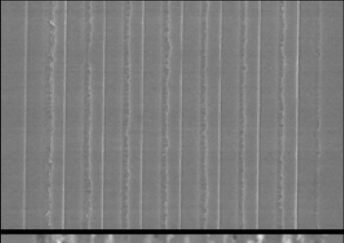
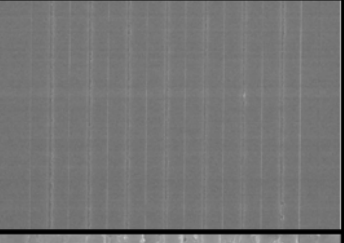
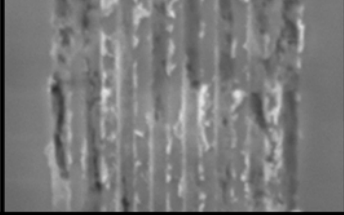
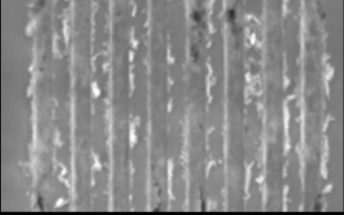
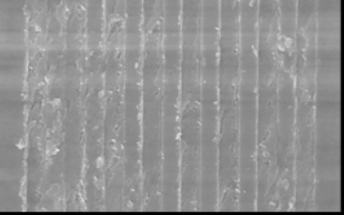
Line width	500 nm	700 nm	1 $\mu$ m
Electroformed Ni mold			
SOG/Ti/Si substrate after 1st annealing			
SOG/Ti/Si substrate after 2nd annealing			

Fig. 22. SEM images of line/ space patterns in electroformed-Ni mold and imprinted SOG substrate before and after the 2nd annealing.

5. Conclusion and future work

An ultrasonic hot embossing was proposed as a new and precise replication technology where the effect of assistance of ultrasonic vibration in hot embossing was experimentally verified. It was found that the contact time and contact force decreased greatly by applying ultrasonic vibration in the molding process. It means that molding in room atmosphere can be carried out under conditions similar to that of vacuum hot embossing. In the marginal cases of hot embossing, the molding rate improved significantly by impressing ultrasonic vibration. Especially, when the contact force was low, the assisting

effect of ultrasonic vibration was quite separate. This phenomenon means that under strong contact force the progression of ultrasonic vibration can be hindered.

Moreover, in order to manage and manipulate the timing at which ultrasonic vibration can be impressed, a system to control the generation of ultrasonic vibration was developed. As for the start time of the impression of ultrasonic vibration set at an earlier stage in the molding process, the assisting effect of ultrasonic vibration was significant.

The effective assistance of ultrasonic vibration in hot embossing was applied to thermal nanoimprinting. Nanopatterns were imprinted on a PC sheet at a temperature close to the  $T_g$  using a thermal nanoimprint system with a built-in ultrasonic vibration unit. And the effect of ultrasonic vibration on thermal nanoimprint was experimentally confirmed. The lowest mold heating temperature in thermal nanoimprint on PC was 165 °C. However, the transfer of all the nanopatterns with the widths of 500 and 750 nm succeeded at a heating temperature of 160 °C using ultrasonic nanoimprint. Thus, it was experimentally shown that nanoimprinting at a low temperature can be done when accompanied by ultrasonic vibration, which can also improve the throughput greatly.

As for the ultrasonic nanoimprint system, its ultrasonic generator was remodeled by substituting a magnetostriction actuator for its piezoelectric actuator. And in one of the results, the imprinted pattern depth at room temperature and without the use of ultrasonic vibration, was found to be as deep as 0.5 mm. However, in the case of ultrasonic nanoimprinting with a contact force of 500 N and contact time of 60 s, the depth of the 1- $\mu$ m-wide pattern reached 1  $\mu$ m. Thus it showed that ultrasonic nanoimprint with the magnetostriction actuator can be used even with PET for a process time of only 1 min. The possibility of greatly improved throughput was experimentally shown by a push-and-pull ultrasonic nanoimprint technology at room temperature.

In the next step, the optimum conditions for ultrasonic nanoimprint on PET were investigated by using the magnetostriction actuator with changeable frequency and amplitude. After that, ultrasonic nanoimprint was applied to six kinds of engineering plastics, and their practicality was confirmed. The depth of imprinted pattern was found to decrease as the  $T_g$  of the plastic rose. The assisting effect of ultrasonic vibration was found to be inversely proportional to the values of  $T_g$ . Moreover, the author developed the ultrasonic nanoimprint technology that enabled room temperature-nanoimprinting of engineering plastics and SOG material.

These experimental results prove that ultrasonic vibration with high frequencies and large amplitudes generate a large amount of frictional heat that can induce drastic thermal-deformation. Therefore, it can be said that ultrasonic nanoimprint is a processing technology that combines plastic deformation by the initial contact force and thermal deformation by ultrasonic vibration. Furthermore, the imprinting limit of our ultrasonic nanoimprint system was also determined. Based on these experimental results, the author is planning to develop a new ultrasonic nanoimprint system capable of generating ultrasonic vibration with higher frequencies and larger amplitudes.

## 6. References

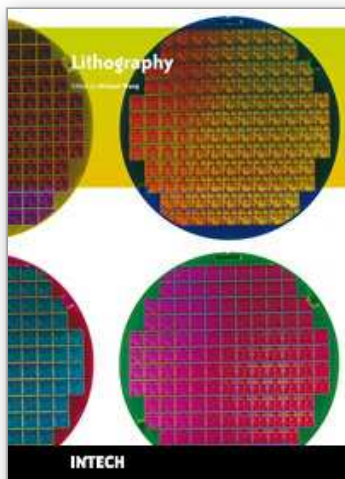
Becker E W; Ehrfeld W; Hagmann P; Maner A & Münchmeyer D. (1986). Fabrication of microstructures with high aspect ratios and great structural heights by synchrotron

- radiation lithography, galvanofforming, and plastic moulding (LIGA process), *Microelectron. Eng.* 4, 35-42.
- Chou S Y; Krauss P R & Renstrom P J (1995). Imprint of sub-25 nm vias and trenches in polymers, *Appl. Phys. Lett.* 67 3114-3116.
- Colburn M; Johnson S C; Stewart M D; Damle S; Bailey T C; Choi B; Wedlake M; Michaelson T; Sreenivasan S V; Ekerdt J & Wilson C G. (1999). Step and flash imprint lithography: a new approach to high-resolution patterning, *Proc. SPIE* 3676 379-390.
- Haisma J; Verheijen M; van den Heuvel K & van den Berg J (1996). Mold-assisted nanolithography: A process for reliable pattern replication, *J Vac. Sci. Technol.* B 14 4124-4128.
- Honeywell International Inc. (2008). Interconnect Dielectrics, Application Note. Publication No. GC0110302Rev2. 3.
- Kishi H; Yoshioka H; Janguo Y; Sumiyoshi N; Goto H; Murakoshi Y & Maeda R. (2003). Thermal Imprinting Stepper with Ultrasonic Vibration Mechanism and Rapid Temperature Control system, *Proc. second International Conference on Nanoimprint Nanoprint Technology* B6.
- Lin C & Chen R. (2006). Ultrasonic nanoimprint lithography: a new approach to nano patterning, *J Microlith. Microfab. Microsyst.* 5 011003.
- Liu S & Dung Y. (2005). Hot Embossing Precise Structure Onto Plastic Plate by Ultrasonic Vibration, *Polym. Eng. Sci.* 45 915-925.
- Maeda R & Ashida K. (2004). Mechanical lithography - State of the Art and the Future, *J Jpn. Soc. Precision Engineering* 70 1219-1222 [in Japanese].
- Maeda R; Goto H; Awazu K; Mekaru H & Takahashi M. (2005). Other nanoimprint technologies, In: *Science & Technology, Essay on Nanoimprint*, Maeda R, (Ed.), 95-107, The Nikkan Kogyo Shimbun, Ltd., ISBN4-526-05574-3, Tokyo [in Japanese].
- Mekaru H; Goto H & Takahashi M. (2006). Development of ultrasonic micro hot embossing technology, *Microelectron. Eng.* 84 1282-1287.
- Mekaru H; Hattori T; Nakamura O & Maruyama O. (2004). Assisted processing of hot embossing by ultrasonic vibration, *Ultrasonic Technol.* 16 66-69 [in Japanese].
- Mekaru H; Nakamura O; Maruyama O & Hattori T. (2004). Development of Precision Transfer Technology of Atmospheric Hot Embossing Replication by Ultrasonic Vibration, *J Soc. Plant Engineers Japan* 16 8-14 [in Japanese].
- Mekaru H; Nakamura O; Maruyama O; Maeda R & Hattori T. (2007). Development of precise transfer technology of atmospheric hot embossing by ultrasonic vibration, *Microsyst. Technol.* 13 385-391.
- Mekaru H; Noguchi T; Goto H & Takahashi M. (2007). Nanoimprint Lithography Combined with Ultrasonic Vibration on Polycarbonate, *Jpn. J Appl. Phys.* 46 6355-6362.
- Mekaru H & Takahashi M. (2008). Ultrasonic Nanoimprint on Poly(ethylene terephthalate) at Room Temperature, *Jpn. J Appl. Phys.* 47 5178-5184.
- Mekaru H & Takahashi H. (2009). Ultrasonic nanoimprint in engineering plastics, *J Vac. Sci. Technol.* A 27 785-792.
- Mekaru H & Takahashi H. (2009). Frequency and amplitude dependencies of molding accuracy in ultrasonic nanoimprint technology, *J Micromech. Microeng.* 19 125026.

- Mekaru H & Takahashi H. (2009). Ultrasonic nanoimprint in Spin-On-Glass (SOG) Coated on Si Substrate, *Jpn. J Appl. Phys. submitted*.
- Motoji T. (2008). Technological trends of fluorine release agents for precise molds, *Tribology* 249 54-56 [in Japanese].
- Schift H. (2008). Nanoimprint lithography: An old story in modern time?. A review, *J Vac. Sci. Technol. B* 26, 458-480.

IntechOpen

IntechOpen



## **Lithography**

Edited by Michael Wang

ISBN 978-953-307-064-3

Hard cover, 656 pages

**Publisher** InTech

**Published online** 01, February, 2010

**Published in print edition** February, 2010

Lithography, the fundamental fabrication process of semiconductor devices, plays a critical role in micro- and nano-fabrications and the revolution in high density integrated circuits. This book is the result of inspirations and contributions from many researchers worldwide. Although the inclusion of the book chapters may not be a complete representation of all lithographic arts, it does represent a good collection of contributions in this field. We hope readers will enjoy reading the book as much as we have enjoyed bringing it together. We would like to thank all contributors and authors of this book.

### **How to reference**

In order to correctly reference this scholarly work, feel free to copy and paste the following:

Harutaka Mekaru (2010). Effect of Applying Ultrasonic Vibration in Hot Embossing and Nanoimprint, Lithography, Michael Wang (Ed.), ISBN: 978-953-307-064-3, InTech, Available from:  
<http://www.intechopen.com/books/lithography/effect-of-applying-ultrasonic-vibration-in-hot-embossing-and-nanoimprint>

**INTECH**  
open science | open minds

### **InTech Europe**

University Campus STeP Ri  
Slavka Krautzeka 83/A  
51000 Rijeka, Croatia  
Phone: +385 (51) 770 447  
Fax: +385 (51) 686 166  
[www.intechopen.com](http://www.intechopen.com)

### **InTech China**

Unit 405, Office Block, Hotel Equatorial Shanghai  
No.65, Yan An Road (West), Shanghai, 200040, China  
中国上海市延安西路65号上海国际贵都大饭店办公楼405单元  
Phone: +86-21-62489820  
Fax: +86-21-62489821



© 2010 The Author(s). Licensee IntechOpen. This chapter is distributed under the terms of the [Creative Commons Attribution-NonCommercial-ShareAlike-3.0 License](https://creativecommons.org/licenses/by-nc-sa/3.0/), which permits use, distribution and reproduction for non-commercial purposes, provided the original is properly cited and derivative works building on this content are distributed under the same license.

IntechOpen

IntechOpen